12-1-2017

PHYSICAL PROPERTIES OF TOPOLOGICAL INSULATOR: BISMUTH SELENIDE THIN FILMS

Yub Raj Sapkota
Southern Illinois University Carbondale, sapkota@siu.edu

PHYSICAL PROPERTIES OF TOPOLOGICAL INSULATOR: BISMUTH SELENID THIN FILMS

By

Yub Raj Sapkota

B.Sc.,Tribhuvan University, 2008
M.Sc., Tribhuvan University, 2012

A Thesis

Submitted in Partial Fulfillment of the Requirements for the

Master of Science

Department of Physics

In the Graduate School

Southern Illinois University Carbondale

December 2017

THESIS APPROVAL

PHYSICAL PROPERTIES OF TOPOLOGICAL INSULATOR: BISMUTH SELENIDE THIN FILMS

By

Yub Raj Sapkota

A Thesis Submitted in Partial

Fulfillment of the Requirements for the Degree of Master of Science

in the field of Physics

Approved by:

Dr. Dipanjan Mazumdar, Chair

Dr. Saikat Talapatra

Dr. K.V. Shajesh

Graduate School

Southern Illinois University Carbondale

July 28, 2017

ABSTRACT OF THE THESIS OF

Yub Raj Sapkota, for the Master of Science degree in Physics, presented on July 28, 2017, at Southern Illinois University Carbondale.

TITLE: PHYSICAL PROPERTIES OF TOPOLOGICAL INSULATOR: BISMUTH SELENIDE THIN FILMS

MAJOR PROFESSOR: Dr. Dipanjan Mazumdar

Topological Insulator (TI) is new classes of materials with gapless surface states and insulating bulk. The topological connection can be traced back to the discovery of Integer Quantum Hall Effect in 1980. In the last decade, new categories of topological insulators were predicted and later discovered, that have gained a lot of attraction for room-temperature applications. Since the experimental observation of single Dirac cone on the surface states of Bismuth selenide (Bi_2Se_3) in 2009, it has emerged as the prototype. Bismuth Selenide has one of the highest bulk band gap of 0.3 eV among all TI materials. While its single crystal properties are well documented, thin films are producing equally exciting discoveries. In this work, Bi_2Se_3 thin films were synthesized using magnetron sputtering method and a diverse set of physical properties, such as structural, optical, and electronic, are investigated. In particular, properties of few-layer (ultra-thin) Bi_2Se_3 thin films are studied. Optical properties of Bi_2Se_3 was particularly revealing. We observed a sharp increase (blue shift) in the bulk band gap of Bi_2Se_3 by almost 0.5 eV as it approached the two-dimensional limit. Strong thickness-dependent structural and transport properties were also observed.

ACKNOWLEDGMENTS

I would like to thank my advisor Dr. Dipanjan Mazumdar for his guidance. He has been a constant source of encouragement. I would like to thank Dr. Saikat Talapatra for serving on my thesis committee and giving feedback on my research. I also would like to thank Dr. K.V Shajesh who taught me advanced quantum mechanics and some theoretical ideas in the field of topological insulators at the beginning of my research and for serving as a thesis committee member.

When I joined the Novel Materials and Heterostructures Laboratory, Hassana Samassekou first introduced me to the experimental part. I would like to thank him for his patience to teach me the basic ideas about the experiments. I am also thankful to Asma Alkabash who provided me with a detailed study of the ellipsometric properties of Bismuth Selenide thin films. Thanks to my colleagues Said Bakkar, Stephen Hofer, and Aaron Walber for their support. I would like to thank Pravin khanal, Sudip Pandey, Anil Aryal, and Prrassana Patil for friendship. I would like to thank the faculty of physics department Dr. Eric Chitamber and Dr. Leo Silbert for teaching me advanced level physics.

Finally, I am grateful to my family: my parents, my brother, and sisters. They are my source of inspiration.

DEDICATION

This thesis is proudly dedicated to

My Parents

TABLE OF CONTENTS

LIST OF TABLES

LIST OF FIGURES

FIGURE PAGE

CHAPTER 1

INTRODUCTION

Topological Insulators [1, 2, 3, 4] are a new quantum state of matter that are different from ordinary insulators. Since 2008, it is a widely researched topic in the field of Condensed Matter Physics and the 2016 Nobel prize was awarded to the pioneers of the concept. Topological insulators (TI) possess an intriguing electrical property. They are metallic on the surface and insulating in the bulk. This makes their band structure also unique and is typified by the existence of an odd number of linearly dispersed Dirac Cones on the surface (see figure 1.1).

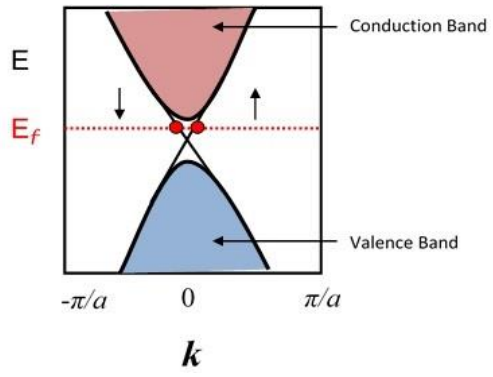

Figure 1.1 Schematic band structure of a topological insulator showing a single Dirac cone that corresponds to the metallic surface state.

This characteristic is robust, meaning that an insulating surface gap opening is prevented (or protected against weak non-magnetic impurities) by time reversal symmetry [5]. This leads to a spin-polarized surface current that travels with very low resistance and no backscattering. TI materials are unique candidates for electronic applications, such as spintronics and quantum computing due to the "dissipation-less" spin-polarized surface currents. As promising as they are, these quantum materials are far from their potential due to other materials-related issues. For example, crystal defects in the form of vacancies and low bulk band gap value (≤ 0.35eV [6] [7])

are recognized to be major roadblocks for device applications for known TIs. Topological states are now considered for diverse device applications such as interconnects [8], low-power devices [9], and thermoelectrics.

The genesis of TIs can be traced back to 1980 with the discovery of integer Quantum Hall Effect (QHE) in 2D electron gas (2DEG) [10]. Under a high magnetic field and at low temperatures, 2DEGs show the quintessential feature of a TI: bulk insulating electron states with metallic edge states that flow in opposite directions. The unique wave function of QHE states is due to the nontrivial topology of the Hilbert Space [11, 12]. This concept can be understood by invoking the language of topology which is a well-known branch in mathematics.

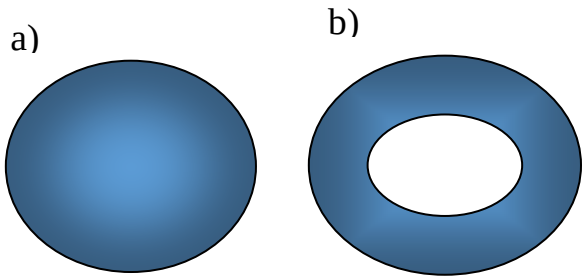

Figure 1.2 The surface of a sphere (g=0) and donut (g=1) are topologically distinct.

The topology of any geometric object can be quantified by its genus. Manifolds with the same number of holes (or genus) can be deformed into one another, but manifolds with different genus (hole) cannot change to other forms. For example, the topology of a sphere is trivial (genus=0) and can be deformed adiabatically into a cube having the same topology (genus=0). But donut, with the genus=1, cannot be deformed adiabatically into the sphere [13]. An object with even number of genus is defined to have a trivial topology and objects with odd number of genus are termed nontrivial. The band structure of common materials can also be classified based on their topological behavior. Materials with even genus number ("trivial") are the conventional materials (e,g, Si, SiO_2) and those with an odd genus number are "nontrivial". In Topological

systems, these nontrivial numbers are known as the Chern numbers which represent the gapless characteristics of the surface due to the closing band gap of the bulk at the interface of a topological insulator and air.

The topological invariant nature of surface state which is represented by a Berry Phase is represented by a TKNN invariant [11]. The surface states Hamiltonian is expressed as,

$$H = v_f (k_x \sigma_y - k_y \sigma_y) \tag{1.1}$$

Where v_f is the fermi velocity and (σ_x, σ_y) are the Pauli matrices, k=(k_x, k_y) is the wave vector [14].

The energy eigenvalues of the Hamiltonian operators are $E = v_f k$ .This gives us the linear dispersion of the Dirac Cone. Due to the Berry curvature at the surface, electrons are moving adiabatically in the unidirectional closed loop which is protected by the time reversal symmetry [15, 16]. Application of a magnetic field or doping with magnetic materials breaks time reversal symmetry. This opens a gap in the surface states. There are other methods to open a surface gap, such as finite-size [17], and is one of the topic of this thesis.

Many applications attempt to utilize the unique attribute of the surface states. It is hypothesized that Majorana fermions, which are massless and are their own antiparticles [18], exists at the interface of topological insulator and superconductor [14]. Majorana fermions are already well known in high energy physics. Due to their non-abelien statistics they can be utilized in fault-tolerating quantum computing [19]. In the next sections, we shall explain the essential theoretical topics of Topological Insulators in some detail such as quantum Hall Effect, Quantum Spin Hall Effect, time reversal symmetry, and spin-orbit coupling.

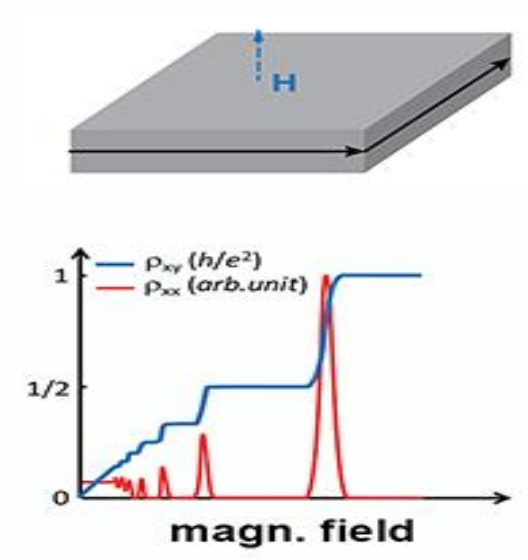

Figure 1.3 The quantum Hall effect (QHE) occurs in a two-dimensional electron system under a large applied magnetic field. Transverse resistivity is quantized and longitudinal resistivity vanishes. [24]

1.1 Theoretical background

As mentioned before, electrons flow along the edges in Quantum Hall systems whereas the conductance of the electron gas in the bulk is zero. The edge states are robust against small perturbation and the direction of the electron will not change due to the presence of weak impurities (figure 1.4). The quantized transverse magneto-conductance, σ_{xy}, is a fractional multiple of $\frac{e^2}{h}$ [10]. This transverse conductance is the property of the bulk. To explain the edge states Thouless, Kohmoto, Nightingale and den Niks proposed a new topological (TKNN) invariant [11]. They modified the transverse magneto-conductance which is given by the TKNN invariant or Chern numbers (C_s) of complete Brillouin zone of the lattice given by,

$$C_s = \int_{BZ} [\vec{\nabla}_k \times \vec{A}^s(k_x, k_y)] d^2\vec{k} \qquad (2.1)$$

Where $\vec{A}^s$ is the berry potential.

Even though the Cherns number seems complicated, Thouless et al. showed that it is precisely the integer in the integer quantized hall conductivity.

After the observation of the Quantum Hall effect, theorists asked whether QHE (Landau Levels) can be observed without the application of magnetic field (i.e, without breaking time reversal symmetry). This was first considered by Haldane in 1988 [20] [21]. Later in 2006, Kane and Mele [22] (and independently by Bernevig and Zhang [23]) extended the Haldane Model and introduced the concept of Z_2 topological insulators and quantum Spin Hall effect. They showed that electrons can move in two opposite directions on the edge without breaking time reversal symmetry in another class of topological invariants called Z_2 (see figure 1.4). The bulk of the material is insulating because of spin-orbit coupling. Such materials show the quantum spin hall effect (quantized spin-Hall conductance and vanishing charge-hall conductance [24]) and are also called 2D topological insulators. For example, Graphene is a candidate QSH Insulator except that the spin-orbit coupling is not strong enough to open a bulk gap.

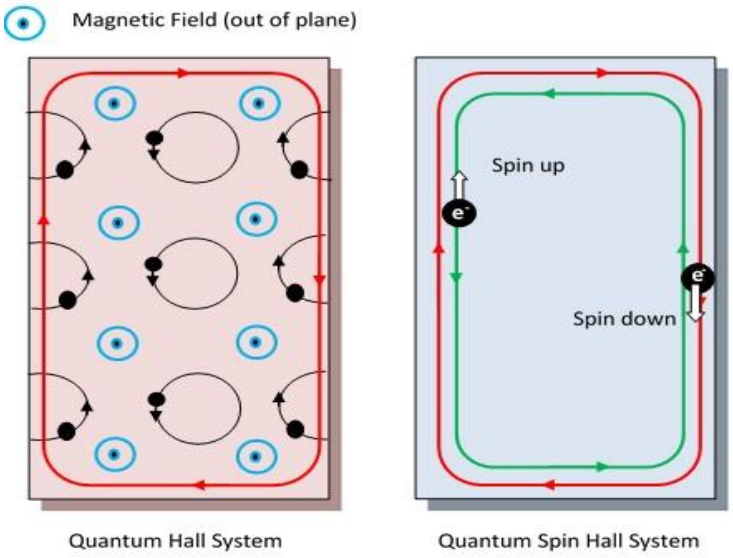

Figure 1.4 Quantum Hall System and Quantum Spin Hall System. Left hand figure: In a Quantum Hall system a magnetic field is required to produce edge states. Right hand figure: No magnetic field is required to generate edge states in quantum Spin Hall System. The spin up (right moving) and spin down (left moving) show linear dispersion (Dirac cone).

1.2 Time Reversal Symmetry

Time Reversal symmetry (TRS) is ubiquitous in physics and plays an integral part in TIs. From elementary physics, we know that physical quantities such as position, density, and Electric field etc. are time reversal invariant because $\mathbf{E}(-t) = \mathbf{E}(t)$. Other quantities such as Magnetic Field, velocity of the particle and Electromagnetic Vector Potential ($\mathbf{A}$) do not conserve TRS. As pointed out before, a magnetic field is not required to observe the edge states in QSH systems, thereby preserving TRS. In Quantum Spin Hall system, electrons are moving clockwise and anti-clockwise direction in two opposite lane to preserve time-reversal symmetry. This trajectory also remains invariant in the presence of non-magnetic impurities. This can be explained in the following manner [25]: In the presence of a non-magnetic impurity, the electron

has two choices. One is to scatter backwards and the other is to move forward (side-ways scattering is not allowed). Figure 1.5 shows the two possible trajectories for backward scattering that involves a π or $-\pi$ rotation around the impurity. This leads to destructive interference [25]. So the back-scattered wave function is always zero, implying the electron can only move in the forward and backscattering is prevented [26]. In the presence of the magnetic impurities, the time reversal symmetry is broken [27].

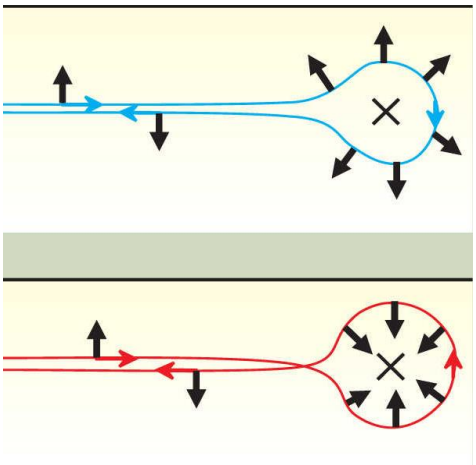

Figure 1.5 Schematic diagram showing back scattering paths in quantum spin hall systems which interfere destructively [25]

1.3 3D Topological Insulators

Topological insulators can be categorized as 2D and 3D type. 2D system with edge states were first predicted theoretically [22] . Topologically, they are characterized by a single non-trivial Z_2 invariant (1,2 etc). Experimentally, 2D topological insulator was first realized in quantum well geometries (CdTe/HgTe/CdTe) [28] and InAs/GaSb/AlSb [29]

Topological properties are also observed in 3D materials (single crystals, etc). Topologically they are characterized by 4 Z_2 invariants (ν_0, (ν_1, ν_2, ν_3)) [5]. Materials with $\nu_0 = 0$

are known as weak 3D TIs. Weak 3D TIs have even number of Dirac cones as the surface states, and net Berry's phase 0 or 2π which are *not* robust with non-magnetic impurity i.e. surface states can be gapped in presence of non-magnetic impurities that break translation symmetry without breaking TRS. Materials with $\nu_0 = 1$ are termed strong TIs. They have odd number of Dirac cones on the surface which is the result of bulk topological order support by the nontrivial Berry's phase of π. Strong topological insulators are robust against the non-magnetic impurity. Bi_xSb_{1-x} single crystals is the first experimentally reported strong 3D Topological insulator with 2D metallic surface states by Heish *et al.* [30] following the prediction by Fu and Kane [31]. Bi_xSb_{1-x} has a complicated band structure with small bulk band gap that varies with x. Later, in 2009, a new set of strong 3D TIs were predicted by Zhang *et al.* using first-principle electronic structure calculation (Sb_2Te_3, Bi_2Se_3, Bi_2Te_3) [32] with a single Dirac cone. The predictions were verified experimentally very soon in Bi_2Se_3 by Xia *et al.* [33] . Bi_2X_3 (X=Se, Te) have a single Dirac cone characterized by the Z_2 topological invariants ($\nu_0 = 1$, (000)). Very soon, other Bismuth and Antimony based layered materials such as Bi_2Te_3 [34] and Sb_2Te_3 [35] were reported. Many other materials demonstrate topological properties such as $TlBiSe_2$, $TlBiTe_2$ and $PbBi_2Te_4$ [36]. Among the known TIs, $TlBiSe_2$ has the largest band gap (0.35 eV) [6] followed by Bi_2Se_3 (0.3 eV). Table 1.1 lists a few known TIs [37].

Apart from single crystals, thin-film growth method is promising for growing high quality TI materials, particularly Bi_2X_3 (X=Se,Te). Molecular-beam epitaxy (MBE) method is proving to be the benchmark in terms of quality (low bulk carriers for example)[38,39,40,41] [38, 39, 40, 41, 42, 43]. Presence of selenium vacancies in thin-films impedes probing of metallic surface states. High bulk carrier concentration ($n_{3D} > 10^{19}$ cm^{-3}) that is typical of Bi_2Se_3 can be lowered during a thin-film growth process [44]. Other methods are also being

explored including Pulsed laser deposition [45] chemical vapor deposition [46] and magnetron sputtering [47]. In this thesis work we clearly demonstrate that magnetron sputtering can be effective in growing TI materials. The thesis work investigates many physical properties of Bi_2Se_3 grown by the magnetron sputtering method.

Table 1.1. A partial list of known Topological insulators. Data from ref [37]

Type	Material	Band gap	Bulk transport	Remark
2D, $\nu = 1$	CdTe/HgTe/CdTe	<10 meV	insulating	high mobility
2D, $\nu = 1$	AlSb/InAs/GaSb/AlSb	~4 meV	weakly insulating	gap is too small
3D (1;111)	$Bi_{1-x}Sb_x$	<30 meV	weakly insulating	complex S.S.
3D (1;111)	Sb	semimetal	metallic	complex S.S.
3D (1;000)	Bi_2Se_3	0.3 eV	metallic	simple S.S.
3D (1;000)	Bi_2Te_3	0.17 eV	metallic	distorted S.S.
3D (1;000)	Sb_2Te_3	0.3 eV	metallic	heavily p-type
3D (1;000)	Bi_2Te_2Se	~0.2 eV	reasonably insulating	ρ_{xx} up to 6 Ω cm
3D (1;000)	$(Bi,Sb)_2Te_3$	<0.2 eV	moderately insulating	mostly thin films
3D (1;000)	$Bi_{2-x}Sb_xTe_{3-y}Se_y$	<0.3 eV	reasonably insulating	Dirac-cone engineering
3D (1;000)	$Bi_2Te_{1.6}S_{1.4}$	0.2 eV	metallic	n-type
3D (1;000)	$Bi_{1.1}Sb_{0.9}Te_2S$	0.2 eV	moderately insulating	ρ_{xx} up to 0.1 Ω cm
3D (1;000)	Sb_2Te_2Se	?	metallic	heavily p-type
3D (1;000)	$Bi_2(Te,Se)_2(Se,S)$	0.3 eV	semi-metallic	natural Kawazulite
3D (1;000)	$TlBiSe_2$	~0.35 eV	metallic	simple S.S., large gap
3D (1;000)	$TlBiTe_2$	~0.2 eV	metallic	distorted S.S.
3D (1;000)	$TlBi(S,Se)_2$	≤0.35 eV	metallic	topological P.T.
3D (1;000)	$PbBi_2Te_4$	~0.2 eV	metallic	S.S. nearly parabolic
3D (1;000)	$PbSb_2Te_4$	?	metallic	p-type
3D (1;000)	$GeBi_2Te_4$	0.18 eV	metallic	n-type
3D (1;000)	$PbBi_4Te_7$	0.2 eV	metallic	heavily n-type
3D (1;000)	$GeBi_{4-x}Sb_xTe_7$	0.1–0.2 eV	metallic	n (p) type at $x = 0$ (1)
3D (1;000)	$(PbSe)_5(Bi_2Se_3)_6$	0.5 eV	metallic	natural heterostructure
3D (1;000)	$(Bi_2)(Bi_2Se_{2.6}S_{0.4})$	semimetal	metallic	$(Bi_2)_n(Bi_2Se_3)_m$ series
3D (1;000)	$(Bi_2)(Bi_2Te_3)_2$	?	?	no data published yet
3D TCI	SnTe	0.3 eV (4.2 K)	metallic	Mirror TCI, $n_M = -2$
3D TCI	$Pb_{1-x}Sn_xTe$	<0.3 eV	metallic	Mirror TCI, $n_M = -2$
3D TCI	$Pb_{0.77}Sn_{0.23}Se$	invert with T	metallic	Mirror TCI, $n_M = -2$
2D, $\nu = 1$?	Bi bilayer	~0.1 eV	?	not stable by itself
3D (1;000)?	Ag_2Te	?	metallic	famous for linear MR
3D (1;111)?	SmB_6	20 meV	insulating	possible Kondo TI
3D (0;001)?	$Bi_{14}Rh_3I_9$	0.27 eV	metallic	possible weak 3D TI
3D (1;000)?	$RBiPt$ (R = Lu, Dy, Gd)	zero gap	metallic	evidence negative
Weyl SM?	$Nd_2(Ir_{1-x}Rh_x)_2O_7$	zero gap	metallic	too preliminary

1.4 Thesis Statement

This thesis work is focused on the growth and physical property investigations of Bi_2Se_3 thin films that include structural, optical and transport properties. Films of different thickness (2-100 nm) were grown using magneto-sputtering technique to study the effect of size on the physical properties. Additionally, the effect of substrate was also investigated in some detail. The optical properties of Bi_2Se_3 as it approaches the 2-dimensional limit was particularly surprising. Using optical absorption spectroscopy, we discovered that ultra-thin films (less than 4 nm) show an increase in the bulk band gap when compared to thicker films (6 nm or higher). Thickness and substrate also had a strong influence on the crystal quality and the transport properties (resistivity, Hall mobility) of the films. The details of these findings are explained in the remainder of the thesis.

1.5 Thesis Outline

In the second chapter, we discuss the properties of Bismuth Selenide and the experimental technique used in this thesis. In Chapter 3, we discuss the structural and transport properties of Bi_2Se_3 films as a function of thickness and substrate. In 4 chapter, we will focus on the optical properties of few-layer Bismuth selenide. Finally, 5 chapter summarizes the major findings of my thesis.

CHAPTER 2

Bi_2Se_3 AND EXPERIMENTAL TECHNIQUES

In this chapter, we discuss the properties of the material of interest (Bi_2Se_3) and the experimental techniques used in the thesis. In section 2.1-2.2 we provide a brief background on Bi_2Se_3 including its finite-size properties. Section 2.3 we provide an overview of the typical synthesis method that is employed to grow Topological materials such as Bi_2Se_3. In section 2.4, we describe the magnetron sputtering method of growing thin films that is used in this thesis work. Structural characterization methods (X-ray diffraction and reflectivity) are discussed in section 2.5. Optical absorption spectroscopy method is briefly discussed in section 2.6. Finally, we describe transport measurement methods in section 2.7.

2.1 Introduction to Bi_2Se_3

Bismuth selenide is a prototypical example among 3D Topological insulators [5]. Single Dirac cone was observed at the Γ point in bulk Bi_2Se_3 through angle-resolved photo emission (ARPES) [16, 15, 33] and scanning tunneling microscopy measurements [48]. It is classified as a strong topological insulator [49], where surface states retain zero-gap despite the presence of atomic-level non-magnetic impurities (very stable even in the presence of strong disorder). The literature has also been growing on Bi_2Se_3 thin films. Recent experiments involving Bi_2Se_3 thin films demonstrated proximity-induced superconductivity [50, 51] and ferromagnetism [52], both phenomena associated with symmetry breaking. Exotic effects such as Quantum anomalous Hall Effect has been experimentally observed in magnetic TI thin films at ultralow temperatures [53, 27, 54].

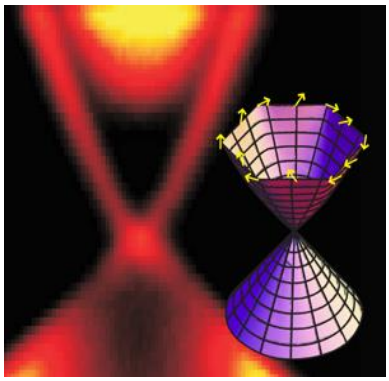

Figure 2 .1 Surface states of Bi2Se3 as measured by ARPES [1]. Clear single Dirac cone is observed.

Bi_2Se_3 has a rhombohedral structure as shown in figure 2.2 belonging to the D^5_{3d} (R-3m) space group. The larger hexagonal unit cell has lattice parameter c= 2.864 nm and a=0.413 nm. The structure can be broken down into covalently bonded Se-Bi-Se-Bi-Se quintuple layer (QL) blocks with a thickness of 0.95 nm**.** Different QLs are held together by weak van-der-Waals bonds.

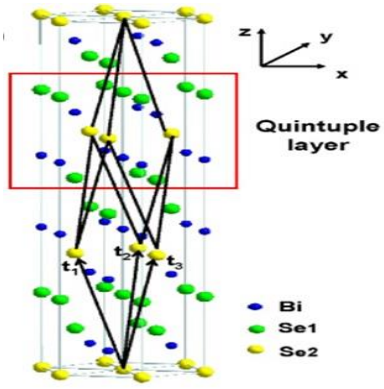

Figure 2.2 Crystal structure of Bi_2Se_3 with three primitive lattice vectors [32]

Among all Bismuth and Antimony-based compound Bismuth Selenide shows one of the highest bulk band gap of 0.3eV [32, 33, 26], In comparison, Bismuth Telluride has a gap of

0.15eV. While ARPES has proved successful in directly imaging the surface properties, transport measurements, that should also probe surface states, are obscured due to large concentration of selenium vacancies in Bi_2Se_3. The vacancies make Bi_2Se_3 strongly n-type doping with a typical bulk carrier concentration of between 10^{18} to 10^{19} cm^{-3}. In comparison, n-doped Si has a carrier concentration between 10^{14}-10^{15} cm^{-3}, and metals have a concentration of 10^{22} cm^{-3}. Even very pure single crystal prepared by Bridgman techniques show high bulk carrier density (>10^{19} cm^{-3}). However, to properly utilize the conducting surface states for device applications, the bulk contribution must be kept low. In this respect, topological properties must survive various tests of scalability and compatibility. Therefore, growth of high-quality TI materials with low defects in thin-film form will provide the platform for further investigations.

2.2. Finite-size properties of Bi_2Se_3

Ultra-thin Bi_2Se_3 is required for exploring nanoelectronics applications. Therefore, scalability of topological properties with reducing thickness is of interest. Theoretically we expect crossover from a 3D TI to 2D TI as the thickness is reduced. Theoretical work indicated that a trivial 2D behavior is possible [55, 56, 57]. i.e., a gapped state due to the hybridization of the top and bottom surfaces. In other words, due to quantum tunneling the top and bottom states talk to each other as the thickness is reduced which opens a surface gap. Experimentally this was observed below the 6 QL in ARPES measurements by Zhang *et al.* [17] as shown in figure 2.3.

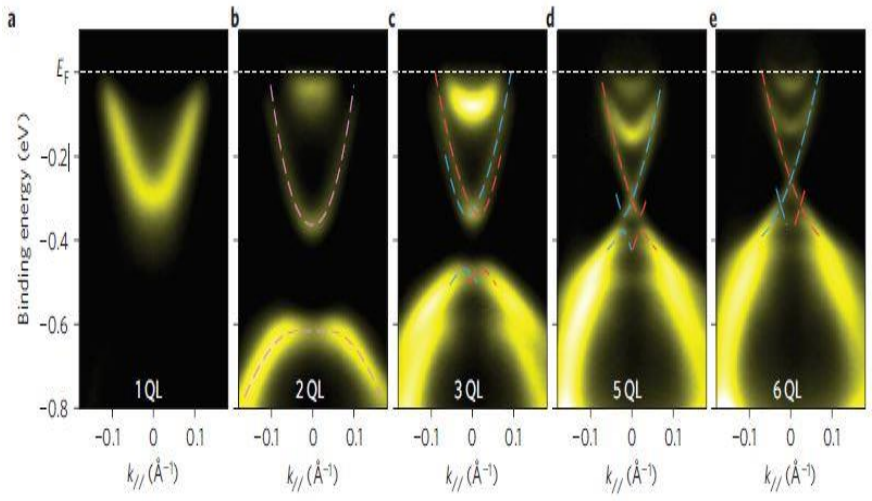

Fig 2.3 Band Gap opening in ultra-thin film bismuth selenide films by using the ARPES. [17]

In short, ultra-thin Bi_2e_3 transforms into to a trivial insulator in the two-dimensional limit. On the positive side, observation of quantum- tunneling modulated spin texture of ultra-thin films open the new door for the possible spin switch nano electronics and spintronic devices application [58]. Insulating behavior was reported in the transport properties of mechanically exfoliated 3 QL films [59] . Recently, first principles density functional theory calculations of 2 QL Bi2Se3 thin films showed increase in the bulk band gap [60]. In the present thesis work, we confirm the increase in bulk gap in the 2D limit through optical spectroscopy. The details are discussed in chapter 4.

2.3 Thin film synthesis of Bi_2Se_3

Popular single crystal synthesis techniques of Bi_2Se_3 and other topological materials are synthesized by Bridgman method, Chemical Vapor Deposition [61] and Physical vapor transport. Mechanical exfoliation of single crystals provides thickness dependent experimental studies of electronic and optical properties [59, 62]. Thin films deposition can be generally classified into either physical or chemical. The well-known method of thin films growth is

Molecular Beam Epitaxy (MBE) which gives high quality epitaxial thin films. Sailent feature of MBE method is a low film growth rate under ultra-high vacuum (UHV) [19, 63, 64, 65, 66, 67]. Growth of Bi_2Se_3 using MBE is reported on different substrates such as Si (111) [64], GaAs (111) [63], $SrTiO_3$ (111) [49], InP (111) [68], CdS (0001) [69], graphene-terminated 6H-SiC(0001) [67] and Sapphire [67]. MBE provides better structural control, sputtering is more versatile, PLD provide better stoichiometry control, and CVD is more cost-effective. Therefore, depending on application, one method might be preferred over other. Thin films of Bismuth Selenide are also synthesized by using magneto-sputtering technique [70] which is a large area growth technique of thin films. Sputtering method is described in detail in the next section as it is the method used in this thesis work. The substrate plays an vital role in the crystal structure of thin films. In our study, we used different substrates such as sapphire, silicon, Si/SiO_2, amorphous Boron nitride buffered Silicon and quartz.

2.4 Physical vapor deposition

Physical vapor deposition (PVD) consists mainly three steps: (1) production of a target atomic, molecular, or ionic species, (2) transport of this material to the substrate through a medium and (3) atomic assembly of the species on the substrate. PVD system is categorize into two: evaporation or sputtering. In the evaporation system the target molecules are evaporated which include molecular beam epitaxy (MBE), Thermal evaporation and laser ablation. The MBE is one of the best way of getting nearly perfect single crystalline structure texture. This system can be used for getting the thin films of metal, semiconductor or insulator. MBE system has relatively very slow growth rate in ultra-high vacuum pressure (10^{-10} torr). This system may be controlled in situ by surface reflection high energy electron diffraction (REED) which is the

unique feature of this system. However, MBE system is very complex and expensive so that it is not preferred for use in large –scale production thin films.

2.4.1 Sputtering

Sputtering system is one of the thin film growth technique in which targeted materials are ejected from the solid source at a higher temperature than its vaporization point [71]. High purity materials are deposited on the substrate in in an Argon environment.

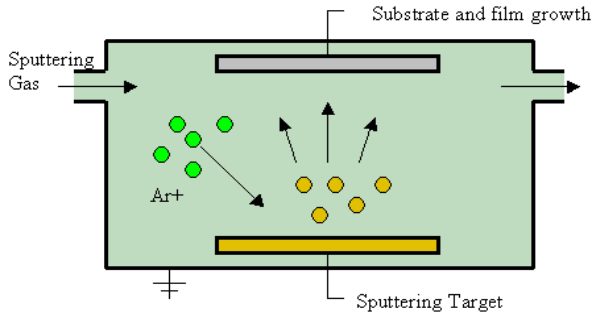

Figure 2.4 A schematic diagram of a typical sputtering system (source: Wikipedia)

An electric field is applied to accelerate the Argon ions present in the chamber. The Argon ions accelerate towards the substrate and sputters the source ingredients from the target in vapor form by a physical momentum-exchange process as shown in figure 2.4. One of the most striking characteristics of sputtering is its universality. Since atoms from the target are by a physical momentum-exchange process, virtually any solid material can be deposited using sputtering process. There are different types of sputtering systems. Among them the DC diode sputtering, RF diode sputtering and DC or RF. Magnetron sputtering is the most advanced technology capable of handling a variety of materials (metals, semiconductors and insulators)

2.4.1.1 Magnetron Sputtering

In our lab, we have the magnetron-sputtering system which is used to fabricate thin films. In this system, a magnetic field is applied parallel to the surface of the target by a pair of planar electrodes, across which a static voltage is applied to create a plasma discharge. The secondary electrons travelling from the target to the substrate are forced into a spiral path due to the Lorentz force. This significantly increases the travel distance of each electron, enhancing the probability of collisions with the background gas atoms. This dramatically increases the impact efficiency of the ejected electrons, making it possible to sputter at lower pressure (1-5 mTorr).

During the deposition of magnetic material attention must be paid. An inhomogeneous magnetic field will result in non-uniform plasma density, which cases non-uniform target erosion and degrades the uniformity of the sputtered films. Figure 2.6 is a photograph of our customized, high-vacuum magnetron sputtering system, which has three targets which can run simultaneously at high temperature, manufactures by AJA international.

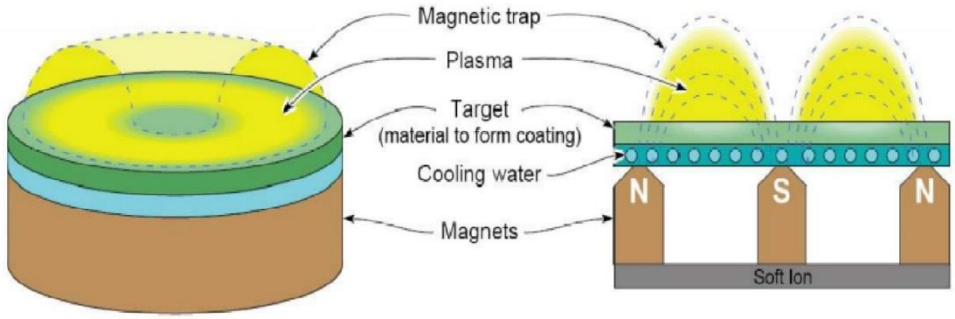

Figure 2.5 Schematic arrangement of the magnets and target in a typical magnetron sputtering system. (source: Wikipedia)

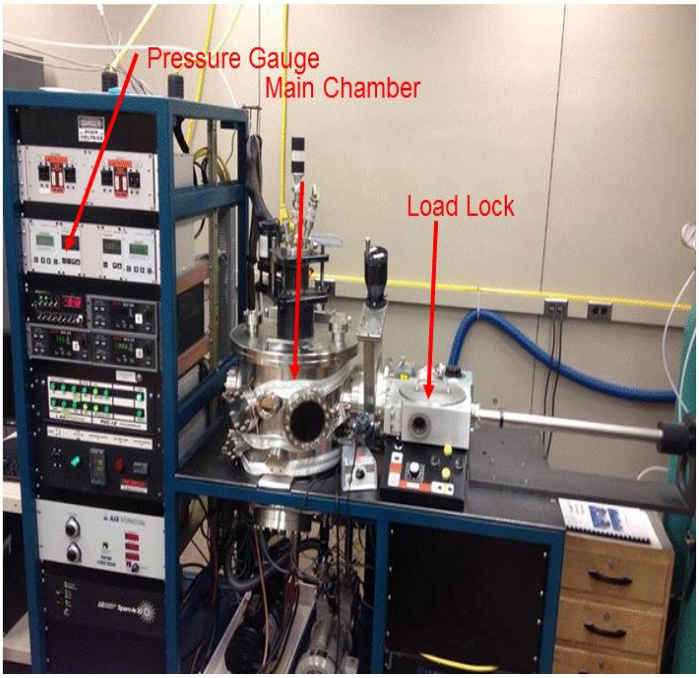

Figure 2.6 Photograph of the magnetron sputtering system in our lab

2.5 Structural characterization

2.5.1. X-ray diffraction

X-ray Diffraction (XRD) is a well-known method to investigate the crystal structure and plane spacing of solid state system. Utilizing the fact that hard X-ray wavelengths comparable to inter-atomic distances, strong diffraction patterns are obtained when X-ray impinge upon a crystal at some specific angles (θ). The distance between the atomic planes (d) is given by the Bragg's law of diffraction.

$$2d\sin\theta = \lambda \qquad (3.1)$$

Where **λ** is the wave length of the X-ray.

The relation between the plane spacing, in plane lattice constant (a), out plane lattice (c) and miller Indies (hkl) for the different lattice are given by

Cubic $$\frac{1}{d^2} = \frac{h^2 + k^2 + l^2}{a^2} \quad (3.2)$$

Hexagonal $$\frac{1}{d^2} = \frac{4}{3}\left(\frac{h^2 + hk + k^2}{a^2}\right) + \frac{l^2}{c^2} \quad (3.3)$$

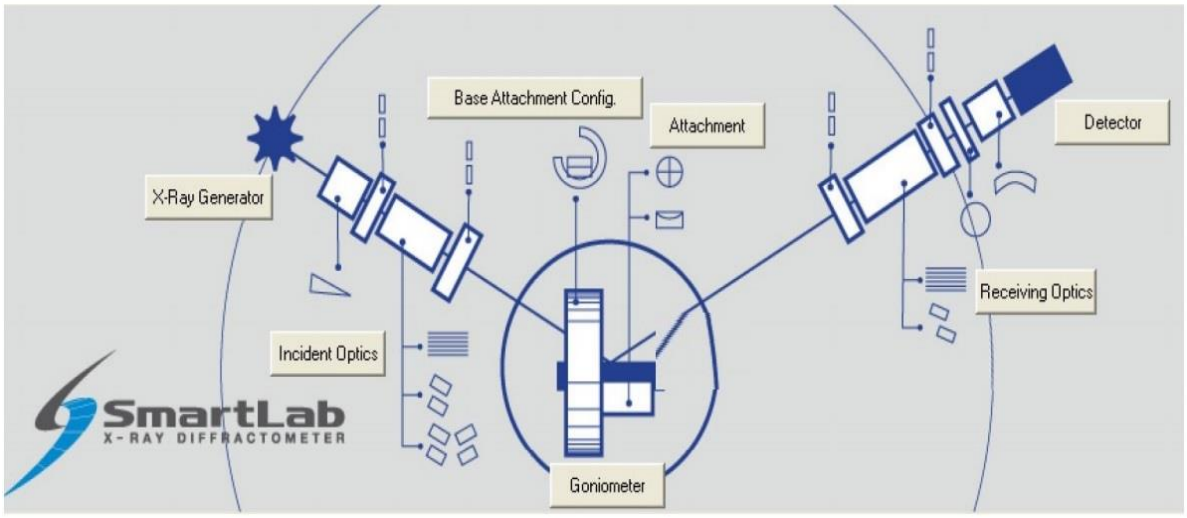

Figure 2.7 Schematic diagram of XRD machine hardware (Source:SmarLab Manual)

Figure 2.7 shows schematic X-ray setup. Cu K-line produced in the X-ray generator is guided using mirrors and slits onto the sample which is placed on the Goniometer. The reflected/diffracted beam is collected by the detector after the beam is conditioned by the receiving optics. Cu produce two K-alpha line and a K-beta line. The K-beta radiation is removed (attenuated) by the Ni filter. $K\alpha_2$ line is removed by a 220-Ge monochromator. Thus

our XRD system (Rigaku Smartlab) produces highly monochromatic $K\alpha_2$ radiation with a wavelength of 1.5404Å. Generally, the out of plane lattice parameter (c-axis) can be extracted easily using a simple two–axis theta-2theta scan when the crystal grows with a preferred (00*l*) orientation. Non-zero h, k, l indices must be exposed to obtain in-plane parameters. It is achieved by four-circle scans (Phi, psi, omega). The texture of the thin films can be measured by rocking curves (omega scans at fixed 2theta).

2.5.2 X-ray reflectivity

X-ray reflectivity (XRR) is a surface sensitive technique that is used to analyze thin films and multi-layers. In a typical XRR scan, X-rays are incident at a grazing angle of incidence and specular reflection from the sample surface is measured. Essentially, it is a theta-2theta scan (like XRD) at very low angles. Various relevant information can be extracted from XRR data such as thickness, large-area roughness, and density values of each individual layer. A simulated XRR pattern for a film (Bi_2Se_3) of a specific thickness and density is shown in figure 2.8.

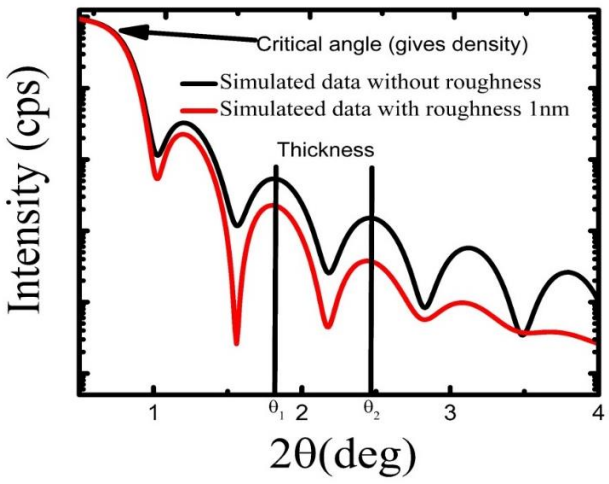

Figure 2.8 Simulated XRR plots for a 13 nm Bismuth Selenide film (density 6.9 gm/cm3) with two roughness values.

At very low angles, X-rays do not penetrate the sample due to total external reflection as density of materials at x-ray wavelengths is slightly less than 1. The critical angle, θc, the angle at which X-rays start to penetrate the sample is related to the density of the underlying layer. Higher θc indicates higher density. For the plot shown in figure 2.8 the critical angle is 2θ ~ 0.8. As the angle increase, the X-rays also reflect from the film-substrate interface and interferes with the top-surface reflection, giving rise to oscillatory interference pattern called Kiessig fringes. The thickness of a single film on a substrate, to a very good approximation, can be calculated from the period of oscillations through the relation

$$t = \frac{\lambda}{2(\sin\frac{\theta_1}{2} - \sin\frac{\theta_2}{2})} \qquad (3.4)$$

Where $\boldsymbol{\theta_2}$ and $\boldsymbol{\theta_1}$ are the angle of consecutive oscillation maxima. This approximation is reliable at angles significantly higher than the critical angle. Another feature of the XRR data is that is sensitive to the RMS roughness of the system. Qualitatively, this can be inferred from the slope of XRR data. As the simulated data of figure 2.8 indicates samples with high roughness loose intensity rapidly with increasing angle. Quantitative estimate can be made through fitting. Multilayers can be analyzed similarly. Parratt's formalism [72] used to extract quantitative data (thickness, roughness, density). and implemented in the simulation software used for this work [73].

2.6 Optical absorption Spectroscopy

Broadband absorption spectroscopy was used to identify the optical band gap and optical property Bi_2Se_3. The measurements covered the near-infrared (NIR), visible (VIS), and ultra-violet range from 190-3300 nm (0.375 eV- 6.2 eV). In a Transmission spectroscopy

measurement setup, the light is incident at normal incidence through a sample (see figure 2.9) and the transmitted light is measured by a detector. The loss of light can be attributed to absorption which in turn can be assigned to the electronic structure of the material under interest. Of course, some of the light is reflected. The relation among transmittance (T), reflectance (R), absorption (α) and thickness (t) of the films for a strongly absorbing medium is given by the relation,

$$T = (1-R)^2 e^{\alpha t} \tag{4.1}$$

This equation is the modified form of Beer's law. For a highly transmitting thin film (particularly on or below the band gap), we can neglect the reflectance and the relation becomes,

$$Absorption(\alpha) = -(\frac{1}{t})\ln T \tag{4.2}$$

This absorption is related to the extinction coefficient (k) by the relation

$$\alpha = \frac{4\pi k}{\lambda} \tag{4.3}$$

The apparatus used is a grating spectrometer, as the wavelength resolution is obtained by using a diffraction grating (Shimadzu UV3600 plus spectrophotometer) as shown in figure 2.9.

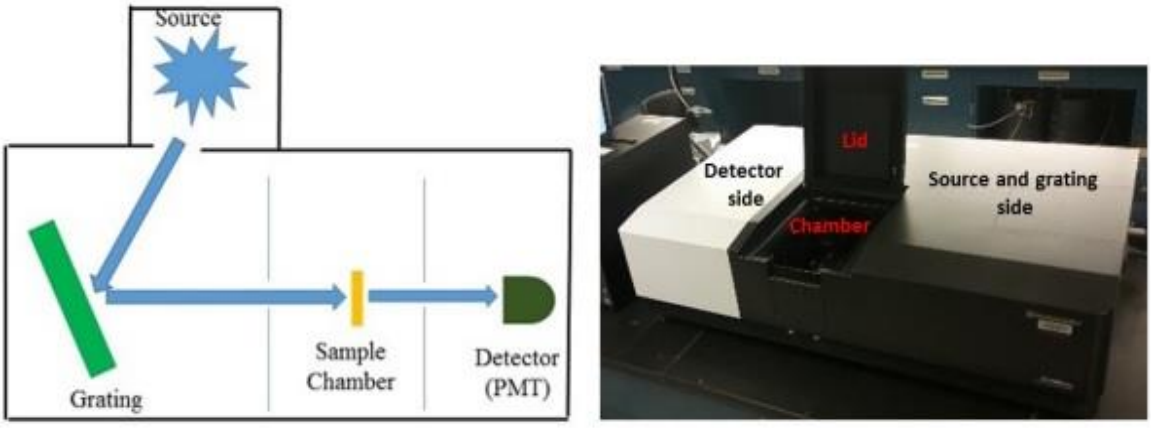

Figure 2.9 Schematic for a NIR-VIS-UV spectrophotometer (left) and Photograph of Shimadzu UV3600 Spectophotometer.

2.7 Transport measurements

Transport measurenebts of Bi_2Se_3 thin-films was carried out in the Van-der-Pauw geometry [74] to measure quantities such as resistivity and Hall mobility. A commercially available setup was used to perform the measurements (NANOMAGNETICS INSTRUMENTS ezhEMS).

2.7.1 Hall effect

Magnetic field is applied perpendicular to the sample during Hall Effect measurement. In this geometry, Lorentz force carries charges towards the edges of the sample until the process stops due to Coulomb repulsion of like charge.

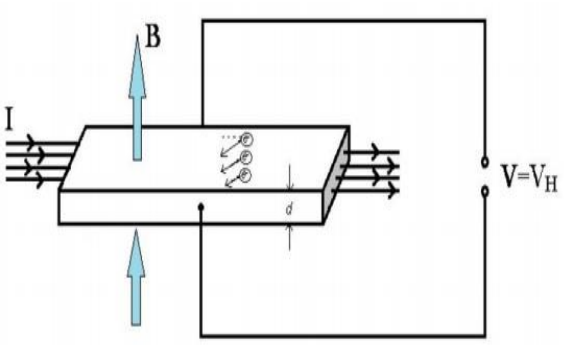

Figure 2.10 A Schematic diagram of the Hall measurement (Source: ezHEMS Manual)

Likewise, at the opposite edge there is a depletion of charges, creating a net voltage called Hall Voltage (V_H) The magnitude of the hall voltage is dependent on the material properties which is given by the equation (5.1)

$$V_H = \frac{IB}{nqd} \tag{5.1}$$

Where I is applied current and B is magnetic field in perpendicular to sample plane, d is the thickness of sample, q is the charge of electron and n is the sheet carrier density.

The Hall coefficient is given by

$$R_H = \frac{1}{nq} = \frac{V_H d}{IB} \tag{5.2}$$

Hall resistance is defined by

$$R_{xy} = \frac{V_H}{I} = \frac{B}{nqd} \tag{5.3}$$

Van-der-Pauw geometries require four-point contacts at the edges of an arbitrary shaped sample. Factors are accurate thickness value and sample uniformity but not sample width nor distance between contacts. However, symmetric geometries as shown in figure 2.11 provide accurate resistivity value.

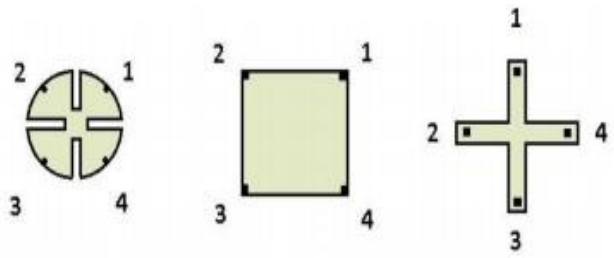

Figure 2.11 Standard van-der-pauw geometries

In our experiment, we employed the square geometry (center figure in 2.12). Current and voltages are measured as described below:

- I_{12} means current is supplied though terminal 1 and taken out from terminal 2.
- $V_{34} = V_3 - V_4$ (5.4)
- $R_{1234} = \frac{V_{34}}{I_{12}}$ (5.5)
- In all Hall measurements, the current is applied along a diagonal (1-3 or 2-4) and the Hall voltage is measured along the other (perpendicular) diagonal.
- Reciprocity dictates that the Hall voltage will be same if we swap the current and voltage terminals.

For an arbitrary shaped material the resistivity is calculated by

$$\rho = \pi t f \frac{R_{1234} + R_{2341}}{2 \ln 2} \quad (5.6)$$

where f is correction factor given by $\frac{R_{1234}}{R_{2341}}$ [74] For our square symmetrical shaped sample

$f = 1$

Hall mobility is given by the relation,

$$\mu = \frac{R_H}{\rho} \quad (5.7)$$

2.8 Conclusion

In this chapter, we described the important properties of Bismuth selenide including its ultra-thin properties. The Magnetron sputtering method of growing Bi_2Se_3 thin films is described in some details. Next, we discussed the structural (x-ray diffraction and reflectivity), optical (absorption spectroscopy), and transport (resistivity and Hall effect) characterization techniques used in this thesis.

CHAPTER 3

STRUCTURAL ANDTRANSPOR PROPERTIES OF Bi_2Se_3 THIN FILMS

In this chapter, we report the structural, and transport properties of topological insulator Bi_2Se_3 thin films grown using magnetron sputtering with emphasis on investigating their dependence as a function of thickness (2-100 quintuple layer) or substrate. In section 3.1, we provide the experimental details on the synthesis of Bi_2Se_3. Section 3.2-3.3 describes the effect of thickness and substrate on the structural properties as investigated through X-ray diffraction and reflectivity. In Section 3.4 we describe their Transport properties.

3.1 Growth of Bi_2Se_3 thin films

Bi_2Se_3 thin films were fabricated in the 2-100 nm thickness range that roughly translates to 2-100 quintuple layers (1 QL ~ 0.95 nm). Growth was performed on different substrates such as $Si/_{SiO2}$ (100 nm), transparent quartz (SiO_2) and amorphous BN-buffered Si, and 001-oriented Si with a native SiO_2 layer, and c-oriented Al_2O_3. Bi_2Se_3 was grown using commercially available stoichiometric target from Kurt Lesker (99.999% purity) and RF sputtered in a high vacuum magnetron sputtering system (base pressure 4×10^{-9} Torr). The growth rate for Bi_2Se_3 was fairly high at 10-15 QL/min even under moderate sputtering power conditions. Films were grown at room temperature and annealed *in-situ* at 300 C. Structural and interface properties were characterized by means of high-resolution X-ray diffraction and reflectivity using a Rigaku Smartlab Diffractometer equipped with a Ge (220) 2-bounce incident bean monochromator to obtain a Cu $K\alpha_1$ radiation. Transport and Hall measurements were done using a NanoMagnetics Instruments ezHEMS system in the Van-der-Pauw (VDP) geometry.

3.2 Effect of thickness on Bi_2Se_3 structure

In figure 3.1 we show the X-ray reflectivity (XRR) pattern of approximately 10-12 QL Bi_2Se_3 films grown on different substrates (Si, Si/SiO_2, amorphous BN, and c-orientated Al_2O_3). XRR is simultaneously a surface and bulk probe technique. An oscillatory pattern is observed in all cases that indicates sharp interface of Bi_2Se_3 with the substrate.

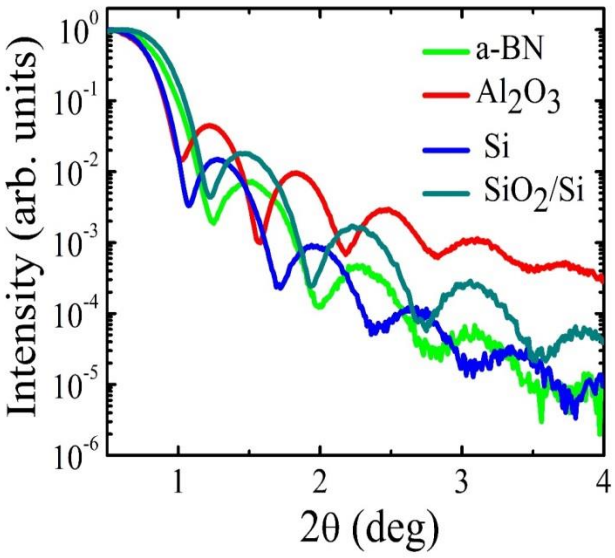

Figure 3.1 we show the X-ray reflectivity (XRR) pattern of approximately 10-12 QL Bi_2Se_3 films grown on different substrates (Si, Si/SiO_2, amorphous BN, and c-orientated Al_2O_3

Analysis of the critical angle reveals that the measured film densities are somewhat higher than the bulk value of ~ 6.8 g/cm^3 by about 15-20 %. Though this value may be within the margin of error, this might also indicate that the films have selenium vacancies (more Bismuth per unit volume) or indication of formation of Bismuth oxide (Bi_2O_3) at the surface which has a much higher density than Bi_2Se_3. The most distinct variation between substrates are the film roughness values that can be inferred qualitatively from the slope of the curves. Fits show that

the film on Al_2O_3 is virtually atomically smooth whereas the film on Si has a roughness of nearly 1 quintuple layer (~0.9 nm). Data on amorphous-BN and SiO_2/Si show intermediate roughness values of 0.7 nm and 0.45 nm respectively.

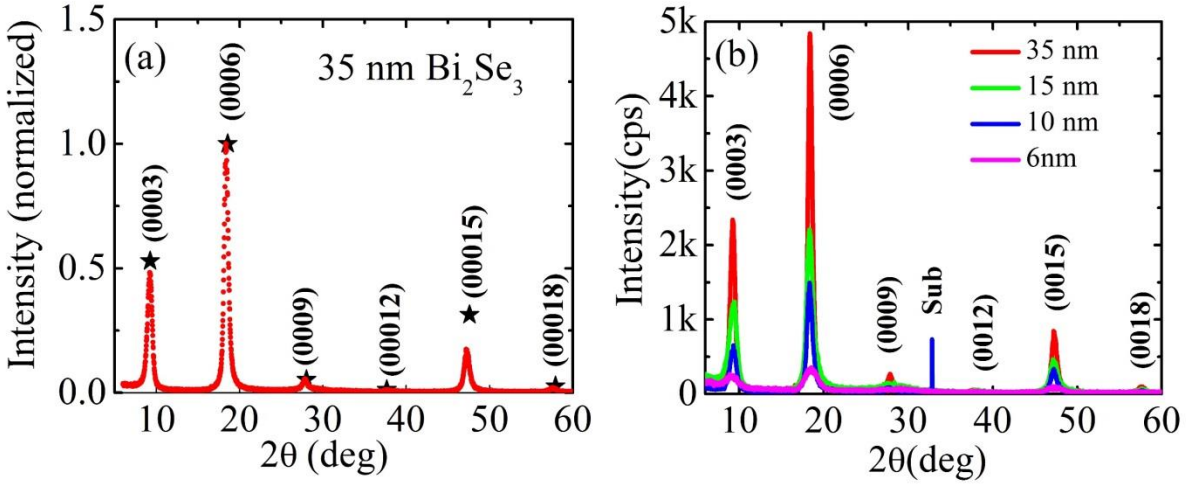

Figure 3.2 (a) Normalized XRD pattern of a 35 nm Bi_2Se_3 film showing only (000l) Bragg peaks. Simulated XRD intensities corresponding to 000l Bragg peaks is shown using black stars. A very good agreement is observed except for the (00015) peak (b) (b) XRD scans of Bi_2Se_3 thin films of different thickness as indicated. 'Sub" indicates substrate peak.

Figure 3.2(a) shows the high resolution θ-2θ XRD pattern of a 35 nm Bi_2Se_3 film deposited on Si/SiO_2 substrate. Various (000*l*) peaks assigned to Bi_2Se_3 are clearly observed. The intensities are normalized with respect to the highest (0006) peak to compare the data to a simulated XRD pattern [75] of bulk Bi_2Se_3 structure (c=28.63 Å) [76] . The (000*l*) simulated peak positions are indicated by black stars. As evident, apart excellent agreement in the Bragg angle, the experimental intensities match simulation very well for all except the (00015) peak, which is somewhat reduced in intensity. This clearly indicates that highly-oriented Bi_2Se_3 films are growing strain-free with bulk-like crystal structure. The oriented crystal structure is also

observed over a wide thickness range. In figure 3.2 b, XRD scans of films of various thickness deposited on SiO_2/Si substrate are shown. Only (000l) peaks are observed down to 6 QL below which some of the low intensity peaks (0009, 00012) fall below the resolution limit of the diffractometer. It is however reasonable to assume that the structural integrity is maintained in films lower than 6 QL thickness. The intensity and Full-Width-Half-Maximum (FWHM) values of the data shown in figure 3.2 b is shown in table 3.1.

Table 3.1 Intensity and Full Wave Half Maxima value of (0006) peaks with thickness

Thickness (nm)	Intensity on Si/SiO_2 (cps)	FWHM (deg)
6	184	1.72
10	1307	0.78
14	1443	0.79
35	3170	0.59

3.3 Effect of substrate on the structure of Bi_2Se_3

X-ray diffraction analysis also show that films deposited on Al_2O_3 possess the best crystallographic structure. In figure 3.3 we show the high-resolution θ-2θ data of 10-12 nm Bi_2Se_3 films deposited on various substrates. Only (000*l*) Bi_2Se_3 peaks are observed on all substrates apart from sharp substrate peaks (indicated by “Sub”) indicating out-of-plane (c-axis) growth in all cases. The film grown on Al_2O_3 (red) shows the highest intensity among all substrates (Figure3.3) whereas the film on amorphous BN (green) shows the lowest XRD

intensity (by almost a factor of five for the (0006) peak). The intensity and FWHM values obtained for all substrates are shown in Table 3.2

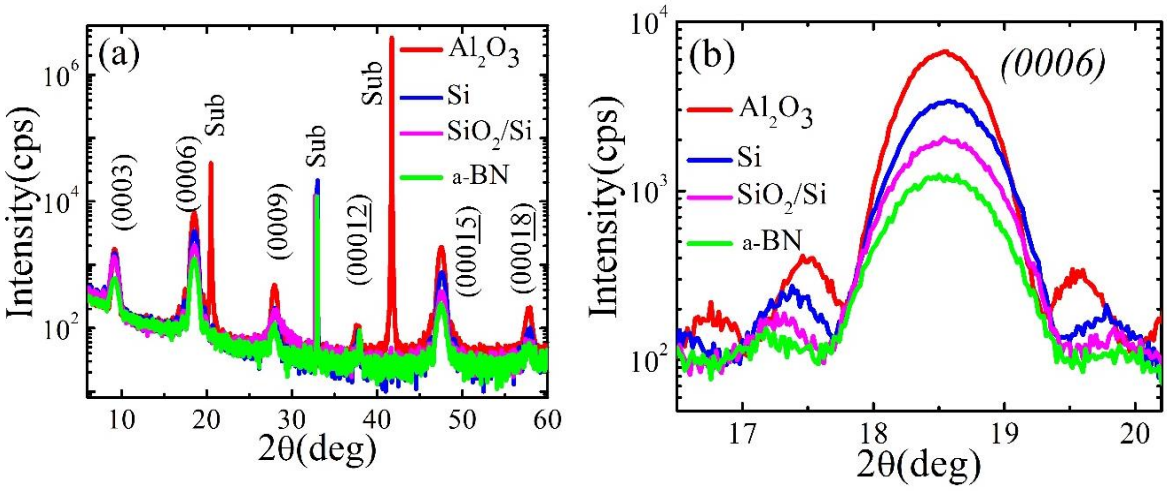

Figure 3.3 (a) X-ray diffraction patterns of 10-12 nm Bi2Se3 films grown on different substrates. "Sub" indicated peaks from various substrates. (b) (0006) peak on different substrates showing variation in intensity. Thickness oscillations are observed around (0006) peak indicating smooth films.

Table 3.2 Intensity (cps) and FWHM value of the (0006) peak as obtained in different substrates

Substrate	Intensity of 10 nm film (cps)	FWHM (deg)
Al_2O_3	4584	0.600
Si	2249	0.726
SiO_2/Si	1307	0.782
BN/Si	792	0.873

Film on SiO_2/Si and Si are of intermediate quality. Similar characteristics are also inferred from the full-width-at-half-maxima (FWHM) value of the (0006) peak from table 3.2. As also clear from figure 3.3b, there is no significant difference in the out-of-plane lattice parameter that indicates that strain effect is not significant in Bi_2Se_3. Therefore, take together with X-ray reflectivity data, our data clearly demonstrate that Bi_2Se_3 films grown on Al_2O_3 have the best topographic and structural quality, consistent with existing reports. Amorphous substrates such as SiO_2 grown in Si are also encouraging and we shall primarily focus on the physical property variation on such amorphous substrates next in the discussion of transport properties.

3.4 Transport properties of Bi_2Se_3: Finite size effects

Transport and Hall effect measurements were performed on exposed Bi_2Se_3 films of various thickness deposited on 1 cm by 1 cm transparent quartz substrates using the Van-der-Pauw method. Quartz substrates were chosen so that the films can be measured for their optical properties simulteneously. In order to minimize surface contamination and aging effect, transport measurements were performed immediately after thin-film deposition. Therefore, new sample were fabricated whenever necessary to improve the accuracy of our measurements. Four-probe ohmic contacts were made by making light contacts with Au/Cr probes onto silver paint deposited at the corners of the square sample. The measurements were completely automated using a LABVIEW program. Samples ranging from thickness of 2-100 QL were employed for this work. Using VDP method, a vast range of parameters such as carrier-type, 2D and 3D carrier concentration, bulk resisitivity, and Hall mobility were analyzed as a functions of thickness at room temperature. These values are summarized in Table 1. We will discuss the relevant parameter next.

Sheet carrier concentration (n_{2D}) shows two distinct regimes. Between 90-15 QL there is a slight reduction in n_{2D} by about a factor of two or three (see Table 3.3). However below 6 QL onwards, we notice a very sharp reduction in n_{2D} values by roughly an order of magnitide as the thickness approaches the two-dimensional limit. The 2QL show much higher sheet resistance which can possibly from poor interface with the amorphous quartz substrate. This is consistent witht the reports of Liu *et al*. [77] where they report similar effects that they attribute to strong electron delocalization and topopolgocal protection.

Bulk carrier concentation (n_{3D}) is largely insensitive to the two-dimensinal effect. It only shows a samller increase (factor three) in the entire 100-2 QL range studied. It is also very in value with concentration of over 10^{19}-10^{20} as shown in Table 3.3. This again points that the bulk carrier concentration is probably dominated by extrinsic factors such as selenium vacancies. Resisitvity values is mostly in the 10^{-3}-10^{-4} range and shows a slight further increase below 6 QL, particularly at the the 2-3 layer range which can be assigned to a quantum confinement effect. Similar insualating behavior has been reported Temperature dependent measurements on 15 and 90 nm film (data not shown) also slow a metalic behavior that is consistent vacancy-induced mobile carrier concentations. Probably the strongest impact of thickness is observed on the Hall mobility values. In figure 3.4 we plot the Hall mobility and the sheet resistance as a fucntion of thickness.

Table 3.3. Carrier concentration (bulk and surface), bulk resistivity, and Hall mobility at 295 K of Bi_2Se_3 thin films of various thickness.n-type behavior was observed in all films

Thickness (nm)	Sheet concentration (cm^{-2})	Sheet resistance (h/e^2 ohm/sq)	Bulk concentration (cm^{-3})	Resistivity (ohm.cm)	Hall Mobility (cm^2/Vs)
90	4.2E+14	--	4.72E+19	0.00108	122
25	2.46E+14	9.5E-3	9.83E+19	6.1E-4	103
15	1.64E+14	2.09E-2	1.09E+20	8.10E-4	70.45
6	9.76E+13	0.1007	1.63E+20	0.00156	24.61
4	6.02E+13	0.2582	2.0E+20	0.002	15.54
3	3.11E+13	0.57147	1.56E+20	0.00295	13.60
2	1.80E+13	7.2391	9.0E+19	0.03737	1.86

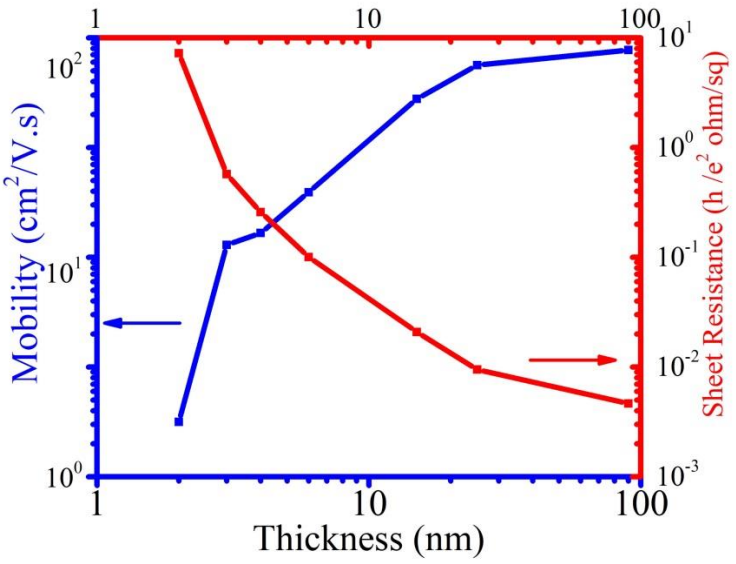

Figure 3.4 Room temperature Hall mobility (blue curve) and sheet resistance (red) of Bi2Se3 thin films grown on quartz substrate. Strong scaling behavior is observed as a function of thickness.

A steep decrease in Hall mobility of nearly two order of magnitude is observed as the thicknes is reduced from 90 nm to 2 nm. This reduction is monotonic but most drastic below 15 nm. Though there is some correlation with inclrease in resistivy value at the 2-3 nm level, it is due to the finite size effect. Its is still not conclusive that what we assume is due to the finite size effect that is coupling of top and bottom layer of the thin films or it is due to the bad interface due to the substrate and bismuth selenide thin films.

3.5 Conclusion

In this chapter, we demonstrate growth of high-quality oriented Bi_2Se_3 thin-films on a variety of substrates including amorphous SiO_2 and BN, with films on isostructural Al_2O_3

substrate exhibiting the best quality. Transport properties reveal a high bulk carrier concentration in all films with n-type behavior and a drastic reduction in two-dimensional carrier concentration and Hall mobility in films below 6 QL thickness. The bulk resistivity of the thin films increased with decrease in thickness.

CHAPTER 4

OPTICAL PROPERTIES OF FEW-LAYER Bi_2Se_3

In this chapter, we shall summarize the optical band gap properties of high-quality few-layer topological insulator Bi_2Se_3 thin films grown in our lab. This work has appeared in a peer-reviewed journal (Yub Raj Sapkota, et al, Applied Physics Letters, **110** 181901 (2017)). We provide direct optical evidence of a blue-shift to up to 0.5 eV in the band gap of Bi_2Se_3 as it approaches the two-dimensional limit. In section 4.1 we briefly motivate the study and survey the optical properties of Bi_2Se_3. In 4.2 we briefly outline the structural properties for few-layer Bi_2Se_3. Section 4.3-4.4 describes the optical properties.

4.1 Introduction to few-layer Bi_2Se_3

Many potential applications of TIs like Bi_2Se_3 will rely on their scaling behavior. It is therefore important and intriguing to ask as to what happens to such exotic materials as they approach the two-dimensional limit? Thin films, therefore, provide an ideal platform to investigate low dimensional physics of TIs. One of the more intriguing consequence of finite-size effects in TIs is the opening of an energy gap in the surface states due to quantum tunneling between the top and bottom surfaces, an effect which was first pointed out by theory [57, 55, 56]**.** and also verified later through first-principles calculations [78, 79]. Experimentally such an effect was directly verified by Zhang *et al* [55]. and Sakamoto *et al*. [80]**.** In ultra-thin Bi_2Se_3 films (below six quintuple layers) through angle resolved photo emission spectroscopy (ARPES) measurement. The observed gap opening is substantially large (~ few tenths of eV). Weak localization effects can also result in a gap opening in few-layer

Bi_2Se_3 thin films, but it is of the order of meV [81]. Also, recently, Vargas *et al.* reported large blue-shift in Bi_2Se_3 nanoparticles, which they attributed to quantum-confinement effects in all directions [62]**.**. All these reports demonstrate that finite-size can have a profound impact in topological materials. In this work, we report that the optical band gap changes can also occur in such materials in the 2-dimensinal limit.

Investigations of optical properties of Bi_2Se_3 thin films has been a subject of previous studies. Variation of optical properties with thickness has also been noted. For example, Post *et al.* [82]**.** studied uncapped 15-99 quintuple layers (QL) Bi_2Se_3 films and found band gap values below 0.3 eV that are attributed to impurity states or surface contamination. Eddrief *et al.* [83]**.** Measured optical properties of 3-54 QL Bi_2Se_3 thin films. While they cover a broad thickness range, the optical properties of the 3 QL film do show a behavior that is consistent, but not clearly reported, with an increase in band gap. Higher optical transmittance in 5 or 6 QL layer Bi_2Se_3 film has been reported that implies higher band gap [84, 85]. However, to the best of our knowledge, a systematic bandgap investigation is lacking at the two-dimensional (few-layer) limit of Bi_2Se_3.

High-quality Bi_2Se_3 few-layer thin films were fabricated in the 2-10 nm thickness range that roughly translates to 2-10 quintuple layers (1 QL ~ 0.95 nm). Bi_2Se_3 was grown using commercially available stoichiometric target and RF sputtered in a high vacuum magnetron sputtering system (base pressure 4×10^{-9} Torr). The structural details are described in Chapter 3. To protect the surface from contamination and oxidation, and yet retain optical transparency in the infrared and visible wavelengths. Some Bi_2Se_3 films were capped with amorphous BN thin films *in situ*.

4.2 Structural properties of ultra-thin Bi_2Se_3

For self-consistency, we shall briefly describe the structural characteristics. Figure 4.1 shows the structural characteristics of an uncapped 10nm Bi_2Se_3 thin film grown on Si/SiO_2 substrate. In figure 4.1, we show the X-ray reflectivity data of the film.

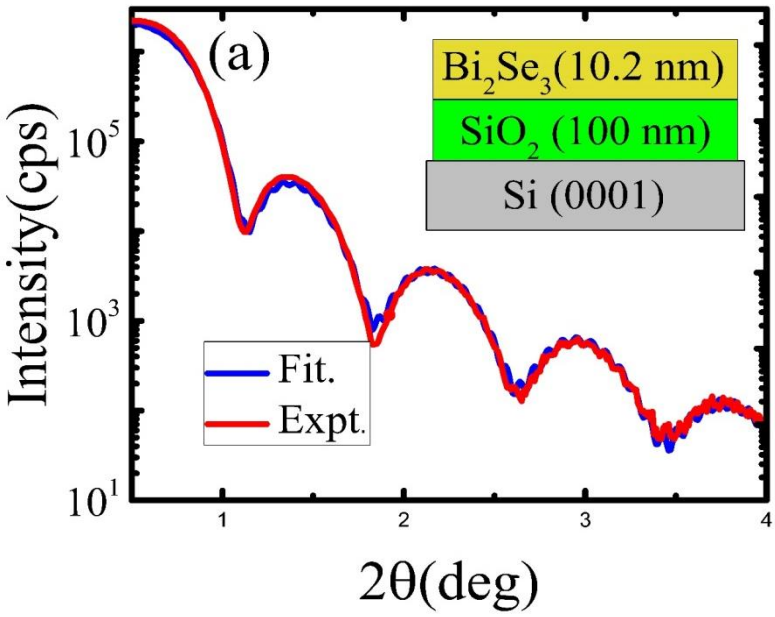

Figure 4.1 High-resolution x-ray reflectivity of ~ 10 nm Bi2Se3 thin film grown on Si/SiO2 substrate. Inset shows the thickness and roughness value of Bi2Se3 film as obtained from the fit of reflectivity data.

Oscillatory thickness pattern from the ~10 nm Bi_2Se_3 layer and the 100 nm SiO_2 layer are observed. This is indicative of sharp interfaces. The thickness and roughness value as obtained from the reflectivity fit [73, 72] is shown in the inset of (Fig4.1). Roughness of ~0.4 nm is less

than half of quintuple layer. The extracted density of the Bi_2Se_3 film is also in very good agreement with bulk value.

Figure 4.2 shows the high-resolution theta-2theta scan of the X-ray diffraction pattern of the 10 QL Bi_2Se_3 thin film. Clear diffraction peaks can be identified for the (002) silicon substrate (labeled as "sub") and (000*l*) peaks of the Bi_2Se_3 layer. This is indicative of out-of-plane growth. Thickness fringes are also observed around the (0003) and (0006) that are consistent with very smooth films. Off-axis measurements on high Miller indices peaks gave a=4.17 Å, c=28.56 Å. Taken together with the reflectivity data, we confirm that the properties of few-layer Bi_2Se_3 films are of superior bulk and interface quality and compares very favorably with Molecular Beam Epitaxy (MBE) grown films.

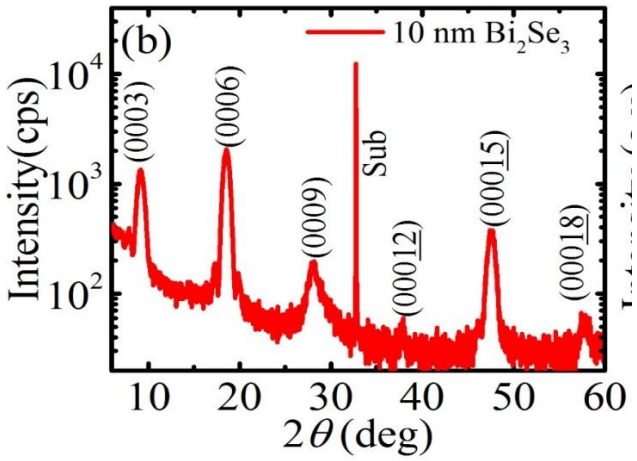

Fig 4.2 X-ray diffraction pattern of 10 nm Bi_2Se_3 film showing only (000l) peaks, implying out of plane growth

4.3 Optical Transmittance measurements

To perform the transmittance measurement, the Bi_2Se_3 samples were deposited on transparent quartz substrates. One set of samples was capped with a few nm of amorphous BN and the other set was left uncapped. Boron nitride is a highly transparent material with a bandgap of 5.5 eV. This allowed us to protect the Bi_2Se_3 layer without affecting its visible and infra-red transmittance. To ascertain the impact of oxidation and other surface changes on the optical characteristics of the films, we measured the transmittance of several capped and uncapped Bi_2Se_3 films at various times after deposition. In figure 4.3 we show the data taken at two times for the 2 QL film which is the thinnest film studied where presumably the oxidation effect, if any, should be the strongest. As expected, the uncapped sample demonstrated some change in its optical transmittance, but it is only a few percent, and mostly in the high-energy range (500-900 nm).

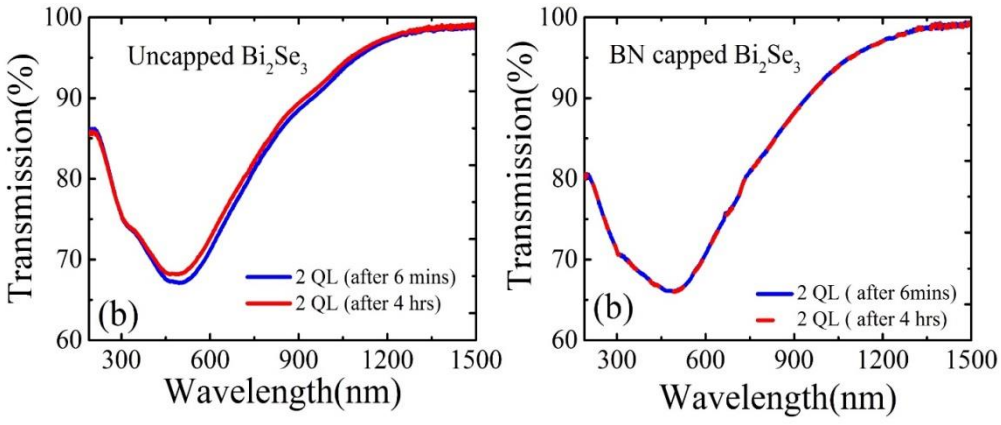

Figure 4.3. Transmittance data of a 2QL uncapped (a) and BN-capped (b) Bi_2Se_3 film taken at different times after film deposition as indicated. The uncapped sample showed only very little variation with time.

The observed change is less than 10% even after 7 days (data not shown), proving that the optical transmittance properties were not affected to any significant degree even at the 2 QL level. The BN capped sample did not show any change as evident from the near-perfect overlap of the data taken after 6 mins and 4 hours. Taken together we infer that even though capping improves reliability, oxidation and other extrinsic effects do not dominate our optical measurements [83]. Encourage by these developments we proceeded to measure the band gap on both types of sample.

4.4 Band-gap spectroscopy of few-layer Bi_2Se_3 thin films

In figure 4.4, we plot the optical absorption as calculated from the transmittance data through the relation $\alpha = -(1/\text{thickness}) * \ln T$.

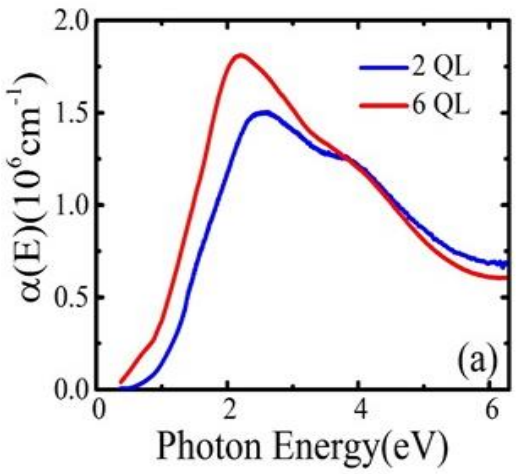

Figure 4.4 Optical absorption data of a 2 and 6 QL Bi2Se3 film showing a blue-shift with inverse thickness

Various optical features can be associated with Bi2Se3. However, the most striking dissimilarity between the two films is the rigid blue-shift in the 2 QL sample compared to the 6 QL data. This clearly indicates that the fundamental band gap of these two systems are

different. The blue-shift in the absorption data continues to up to 3.5 eV, above which the optical properties overlap reasonably well. To quantify the optical band gaps accurately, we plot the $(\alpha E)^2$ vs the photon energy (Fig. 4.5) to reveal the direct gaps of few-layer Bi_2Se_3.

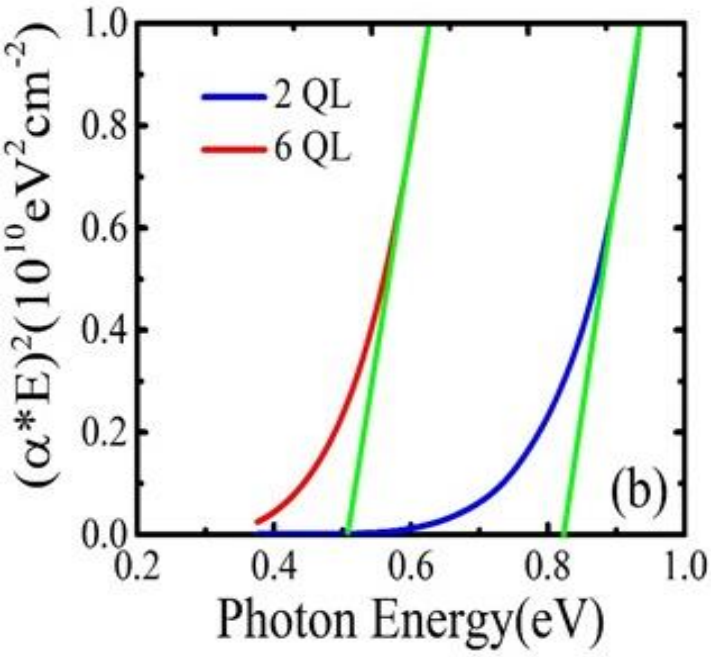

Figure 4.5 Direct Band gap analysis

Though this method was developed to measure optical properties of semiconductors with parabolic bands it has often been extended (successfully) to other systems. The measured band gap for the 2QL film is ~0.8 eV whereas the value for the 6QL film is ~0.5 eV. In figure 4.6, we plot the band gaps of all the few-layer films (both capped and uncapped). The strong in increase in band gap with decreasing thickness is seen in both types of samples. The obtained band gap for the 15 QL film is close to bulk value (~0.3 eV), that demonstrates that the systematic error in the band gap estimation is small, if any (less than 0.1 eV).

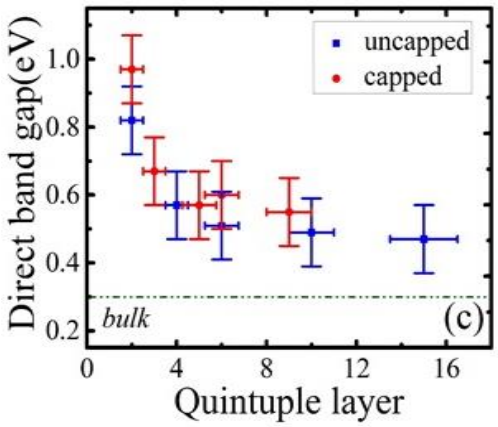

Figure 4.6. The direct band gap for films of different thickness. Both capped and uncapped films follow the same trend of increasing band gap with inverse thickness below 6 QL.

Our observations are consistent with strong differences in the electronic character of two-dimensional Bi_2Se_3 compared to bulk. Previous efforts have highlighted that finite size effect is particularly important when the top and bottom surfaces starts to interact with each other, the onset of which starts below six QL. It is therefore not a coincidence that the most significant bulk band gap change is for thicknesses below six quintuple layers. Very recent first principle calculation also conform this result [60]. We therefore hypothesize while optical transmittance measurements might not be directly sensitive *only* to the surface states, we are indirectly measuring the effects of it. It is also worth noting that Vargas *et al.* reported a theoretical band gap of ~0.8 eV for a 2QL Bi_2Se_3 [62], which is also in excellent quantitative agreement with our results. Therefore, we conjecture that quantum confinement effects might already play a significant role at the 2D level. Additional lateral confinement will only amplify this effect. At present, we have not confirmed this effect for a single Bi_2Se_3 layer but believe that it will be a robust effect.

Another important observation is that the bandgap values of thicker films (10 QL or more) are considerably larger than the reported bulk value by about 0.2 eV. We explained this as due to the Burstein-Moss (BM) effect, which is observed in semiconductors with high carrier concentration (> 10^{18} cm^{-3}) [86]. In such cases, the Fermi level moves to the conduction band and results in an apparent increase in the bandgap due to Pauli blocking of occupied conduction band (CB) states. Preliminary Hall effect studies on our 10-30 QL films revealed a carrier concentration more than 10^{19} cm^{-3} which is typical of Bi_2Se_3 [87].

4.5 Conclusion

In conclusion, we have provided optical evidence of a bulk blue shift in Bi_2Se_3 thin films as we approach the two-dimensional limit. High-quality, oriented, few-layer Bi_2Se_3 films was grown using magnetron sputtering and their structural and optical properties were investigated using transmittance spectroscopy. Up to 0.5 eV change in band gap is observed, and most significantly below 6 QL. The effect is robust and is observed in both capped and uncapped films. We explain the increase through a combination of finite-size and Burstein-Moss effect. Overall, our data sheds more evidence into the scaling behavior of TI systems that can potentially have interesting consequences in future nanoelectronics devices. The increase in band gap from 0.3 eV to nearly 1.0 eV also can be utilized in opto-electronic areas such as photodetector and solar cells.

CHAPTER 5

SUMMARY

In this work, high-quality, oriented, Bi_2Se_3 films were grown using ultra-high vacuum magnetron sputtering system and their structural (X-ray diffraction, X-ray reflectivity), transport (resistivity, Hall mobility) and optical (absorption spectroscopy) properties was investigated. Films of various thickness (2-100 nm) were grown on a varitey of subtrates such as Si, SiO_2 (100 nm)/Si, saphhire, amorphous BN buffered Si, and transparent quartz. X-ray diffraction scans demonstrated the growth of high-quality films with lattice parameter very close to single crystals. The structual quality was verified down to a few-layers. The best crystal structure was observed on sapphire substrate which has a compatible structure with Bi_2Se_3, followed by Si, a-SiO_2/Si and a-BN/Si. X-ray reflectivity measurements also demonstrated that films on sapphire were the smoothest with sharp film-sustrate interface. Typical roughness values were as low as 0.4 nm. The weakly bonded nature of van-der-waals force between the substrate and Bismuth selenide layer allowed us to succesfully achieve high quality growth of Bi_2Se_3 thin films on different substrates.

The transport results suggest an n-type behavior with high carrier concentration which is attributed mainly to Selenium vacancies and low bulk band gap. Van der Paw measurements reveled a carrier concentration greater than 10^{19} cm^{-3} regardless of the thickness of the sample which is indicative of degenerate semiconducting behavior. Both Hall mobilty and resistivity showed very strong scaling behvior with thickness. Hall mobility decreased two orders of magnnitude while resisitivty increased two orders as the thickness was reduced from 100 nm to 2nm.

We observed optical evidence for a bulk blue shift in Bi_2Se_3 thin films as we approached the two-dimensional limit. Up to 0.5 eV change in band gap is observed, and most significantly below 4 nm. The effect is robust and was not affected by exposure to ambient conditions even for the thinnest film studied (2nm). We explain the increase through a combination of two factors. Firstly, it is well documented that in the 2D limit Bi_2Se_3 turns into topological insulator with gapped surface states due to quantum interference of the top and bottom surface states. Our optical measurements suggest that there is also a bulk gap change as the surface states are gapped probably due to hybridization effects. This explains the band gap difference (0.3 eV) between the 2 and 6 nm films. This observation is also confirmed by first-principles calculations. Furthermore, we observed that bulk-like films (greater than 10 nm) also show a high band gap (~0.5 eV rather than the expected value of 0.3 eV). We explain this is due to Burstein-Moss effect. Due to the high carrier concentration, the low-lying conduction band states are occupied and the Fermi level is pushed to the conduction band. As a result the apparent optical band gap is increased. Prior ARPES and transport data is consistent with our data. This work opens up an array of optical applications for Bi_2Se_3 thin films.

REFERENCES

[1] M. Z. Hasan, "Viewpoint: Berry's phase and quantization in topological insulators," *Physics,* vol. 3, p. 62, 2010.

[2] N. Nagaosa, "A New State of Quantum Matter," *Science,* vol. 318, no. 5851, pp. 758-759, 2007.

[3] M. Z. Hasan and C. L. Kane, "Colloquium: Topological insulators," *Rev. Mod. Phys.,* vol. 82, p. 3045, 2010.

[4] M. Hasan and C. Kane, "Colloquium: Topological insulators," *Rev.Mod.Phys.,* vol. 83, pp. 1057-1110, 2011.

[5] L. Fu, C. L. Kane and E. J. Mele, "Topological Insulators in Three Dimensions," *Phys. Rev. Lett.,* vol. 98, p. 106803, 2007.

[6] T. Sato, K. Segawa, H. Guo, K. Sugawara, S. Souma, T. Takahishi and Y. Ando, "Direct Evidence for the Dirac-Cone Topological Surface States in the Ternary Chalcogenide TlBiSe2," *Phys.Rev. Litt.,* vol. 105, p. 136802, 2010.

[7] T. Sato, K. Segawa, K. Kosaka, S. Souma, K. Nkayama, K. Eto, T. Minami, Y. Ando and T. Takahashi, "Unexpected mass acquisition of Dirac fermions at the quamtum phase transition of a topological insulator," *Nat. Phys.,* vol. 7, pp. 840-844, 2011.

[8] M. T. Philip, M. R. Hirsbrunner, M. J. Park and M. J. Gilbert, "Performance of topological insulator inerconnects," *IEEE Electron Device Letters*, vol. 138, 2017.

[9] S. K. Banerjee, L. F. Register, E. Tutuc, D. Reddy and A. H. MacDonald, "Bilayer PseudoSpin Field-Effect Transistor (BISFET): A Proposed New Logic Device," *IEEE Electron Device Letter*, vol. 30, p. 158, 2009.

[10] K. Klitxing, G. Dorda and M. Pepper, "New Method for High-Accuracy Determination of the Fine-Structure Constant Based on Quantized Hall Resistance," *Phys. Rev. Lett.,* vol. 45, p. 494, 1980.

[11] D. J. Thouless, M. Kohmoto, M. P. Nightingale and M. Nijs, "Quantized Hall Conductance in a Two-Dimensional Periodic Potential," *Phys. Rev. Lett.,* vol. 49, p. 405, 1982.

[12] A. P. Schnyder, S. Ryu, A. Furusaki and A. W. W. Ludwig, "Classification of topological insulators and superconductors in three spatial dimensions," *Phys. Rev. B,* vol. 78, p. 195125, 2008.

[13] M. (. Franz and L. (. Molenkamp , Topological Insulators (Contemporary Concepts of Condensed Matter Science), Elsevier, 2013.

[14] G. Rosenberg, "Surface magnetic ordering in topological insulators with bulk magnetic dopants," vol. 85, no. 195119, 2012.

[15] D. Hsieh, Y. Xia, D. Qian, L. Wray, J. Dil, F. Meier, J. Osterwalder, L. Patthey, J. Checkelsky, N. Ong, A. Fedrov, H. Lin, A. Bansil, D. Grauer, J. Cava and M. Hasan, "A tunable topological insulator in the spin helical Dirac sransport regime," *Nature,* vol. 460, p. 096407, 2008.

[16] X.-L. Qi and S.-C. Zhang, "Topological insulators and superconductors," *Rev. Mod. Phys.*, vol. 83, p. 1057–1110, 2011.

[17] Y. Zhang, K. He, C.-Z. Chang, C.-L. Song, L.-L. Wang, X. Chen, J.-F. Jia, Z. Fang, X. Dai, W.-Y. Shan, S.-Q. Shen, Q. Niu, X.-L. Qi, S.-C. Zhang, X.-C. Ma and Q.-K. Xue, "Crossover of the three-dimensional topological insulator Bi2Se3 to the two-dimensional limit," *Nature Physics,* vol. 6, p. 584, 2010.

[18] E.Majorana, *Cimento,* vol. 14, p. 171, 1937.

[19] X. Chen, X.-C. Ma, K. He, J.-F. Jia and Q.-K. Xue, "Molecular Beam Epitaxial Growth of Topological Insulators," *Adv. Mater.*, vol. 23, no. 9, p. 1162–1165, 2011.

[20] F. D. M. Haldane, "Model for a Quantum Hall Effect without Landau Levels: Condensed-Matter Realization of the "Parity Anomaly"," *Phys. Rev. Lett.*, vol. 61, p. 2015, 1988.

[21] S. Murakami, N. Nagaosa and S.-C. Zhang, "Dissipationless Quantum Spin Current at Room Temperature," *Science,* vol. 301, no. 1087128, pp. 1348-1351, 2003.

[22] E. J. Mele and C. L. Kane, "Quantum Spin Hall Effect in Graphene," *Phys. Rev. Lett.*, vol. 95, p. 146802, 2005.

[23] B. A. Bernevig and S.-C. Zhang, "Quantum Spin Hall Effect," *Phys. Rev. Lett.,* vol. 96, p. 106802, 2006.

[24] K. He, "Viewpoint: The Quantum Hall Effect Gets More Practical," *Physics,* vol. 8, p. 41, 2015.

[25] X.-L. Qi and S.-C. Zhang, "The quantum spin Hall effect and topological insulators," *Physics Today*, vol. 63, no. 1, p. 33, 2010.

[26] T. Zhang, P. Cheng, X. Chen, J.-F. Jia, X. Ma, K. He, L. Wang, H. Zhang, X. Dai, Z. Fang, X. Xie and Q.-K. Xue, "“Experimental Demonstration of Topological Surface States Protected by Time-Reversal Symmetry," *Phys. Rev. Lett.,* vol. 5, pp. 398-402, 2009.

[27] J. G. Checkelsky, R. Yoshimi, A. Tsukazaki, K. S. Takahashi, Y. Kozuka, J. Falson, M. Kawasaki and Y. Tokura, "Trajectory of the anomalous Hall effect towards the quantized state in a ferromagnetic topological insulator," *Nature Physics,* vol. 10, p. 731, 2014.

[28] M. König, S. Wiedmann, C. Brüne, C. Roth, H. Buhmann, L. W. Molenkamp, X.-L. Qi and S.-C. Zhang, "Quantum spin hall insulator state in HgTe quantum wells," *Science,* vol. 318, no. 5851, pp. 766-770, 2007.

[29] C. Liu, T. L. Hughes, X.-L. Qi, K. Wang and S.-C. Zhang, "Quantum Spin Hall Effect in Inverted Type-II Semiconductors," *Phys. Rev. Lett.,* vol. 100, p. 236601, 2008.

[30] D. Hsieh, D. Qian, L. Wray, Y. Xia, Y. Hor, R. J. Cava and M. Z. Hasan, "A topological Dirac insulator in a quantum spin Hall phase," *Nature,* vol. 452, p. 970, 2008.

[31] L. Fu and C. L. Kane, "Topological insulators with inversion symmetry," *Phys. Rev. B*, vol. 76, p. 045302.

[32] H. Zhang, C. Liu, X. Qi, H. Dai, S. Zhang, Z. Fang and S.-C. Zhang, "Topological insulators in Bi2Se3, Bi2Te3 and Sb2Te3 with a single Dirac cone on the surface," *N. Phys.*, vol. 5, pp. 438 - 442, 2009.

[33] Y. Xia, D. Qian, D. Hsieh, L. Wray, A. Pal, H. Lin, A. Bansil, D. Grauer and Y. S. Hor, "Observation of a Large-Gap Topological-Insulator Class sith a Single Dirac Cone on the Surface," *Nat. Physics*, vol. 5, pp. 398-402, 2009.

[34] Y. L. Chen, J. A. Analytis, J.-H. Chu, Z. K. Liu, S.-K. Mo, X. L. Qi, H. J. Zhang, D. H. Lu, X. Dai, Z. Fang, S. C. Zhang, I. R. Fisher, Z. Hussain and Z.-X. Shen, "Experimetnal Realization of a Three-Dimensioanl Topological Insulator, Bi2Te3," *Science*, vol. 325, no. 5937, pp. 178-181, 2009.

[35] D. Hsieh, Y. Xia, D. Qian, W. F. Meier, J. H. Dil, J. Osterwalderr, L. Patthey, A. V. Fedorov, H. Lin, A. Bansil, D. Grauer, Y. S. Hor, R. J. Cava and M. Z. Hasan, "Observation of Time-Reversal-Protected Singel-Dirac-Cone Topological-Insulatr States in Bi2Se3 and Sb2Te3," *Phys. Rev. Lett.*, vol. 103, p. 146401, 2009.

[36] K. Kuoda, H. Miyahara, M. Ye, S. V. Eremeev, M. Y. Moriyoshi, E. E. Krasovskii, E. V. Chulkov, S. Hiramoto, C. Moriyoshi, Y. Kuroiwa, K. Miyamoto, T. Okuda, M. Arita, K. Shimada, H. Namatame, M. Taniguchi, Y. Ueda and A. Kimura, "Experimental Verification of PbBi2Te4 as a 3D Topological Insulator," *Phys. Rev. Lett.,* vol. 108, p. 206803, 2012.

[37] Y. Ando, "Topological Insulator Materials," *J. Phys. Soc. Jpn.,* vol. 82, p. 102001, 2013.

[38] C. L. Song, Y. Wang, Y. Jiang, Y. Zhang, C. Chang, L. Wang, K. He, X. Chen, J. Jia, Y. Wang, Z. Fang, X. Dai, X. Xie, X. Qi, S. C. Zhang and Q. Xue, "Topological insulator Bi2Se3 thin films grown on double-layer graphene by molecular beam epitaxy," *Applied Physics Letters,* vol. 97, p. 143118, 2010.

[39] X. F. Kou, L. He, F. X. Xiu, M. R. Lang, Z. M. Liao, Y. Wang, A. V. Fedorov, X. X. Yu, J. S. Tang, G. Huang, X. W. Jiang, J. F. Zhu, J. Zou and K. L. Wang, "Epitaxial growth of high mobility thin films on CdS," *Applied Physics Letters,* vol. 98, p. 242102, 2011.

[40] A. A. Taskin, S. Sasaki, K. Segawa and Y. Ando, "Manifestation of Topological Protection in Transport Properties of Epitaxial Bi2Se3 Thin Films," *Physical Review Letters,* vol. 109, p. 066803, 2012.

[41] T. P. Ginley, Y. Wang and S. Law, "Topological Insulator Film Growth by Molecular Beam Epitaxy: A Review," *Crystals,* vol. 6, p. 154, 2016.

[42] H. D. Li, Z. Y. Wang, X. Kan, X. Guo, H. T. He, Z. Wang, J. N. Wang, T. L. Wong, N. Wang and M. H. Xie, "The van der Waals epitaxy of Bi2Se3 on the vicinal Si(111) surface: an approach for preparing high-quality thin films of a topological insulator," *New Journal of Physics,* vol. 12, p. 103038, 2010.

[43] Y. Guo, Z. Liu and H. Peng, "A Roadmap for Controlled Production of Topological Insulator Nanostructures and Thin Films," *Small,* vol. 11, p. 3290, 2015.

[44] B. C. Park, T. Kim, K. I. Sim, B. Kang, J. W. Kim, B. Cho, K. Jeong, M. Cho and J. H. Kim, "Terahertz single conductance quantum and topological phase transitions in topological insulator Bi2Se3 ultrathin films," *Nature Communications,* vol. 6, p. Article number: 6552, 2015.

[45] P. Orgiani, C. Bigi, P. K. Das, J. Fujii, R. Ciancio, B. Gobaut, A. Galdi, C. Sacco, L. Maritato, P. Torelli, G. Panaccione, I. Vobornik and G. Rossi, "Structural and electronic properties of Bi2Se3 topological insulator thin films grown by pulsed laser deposition," *Applied Physics Letters,* vol. 110, p. 171601, 2017.

[46] Y. Lin, Y. Chen, C. Lee, J. Wu, H. Lee, C. Liang and Y. Chang, "A study on the epitaxial Bi2Se3 thin film grown by vapor phase epitaxy," *AIP Advances,* vol. 6, p. 065218, 2016.

[47] W. J. Wang, K. H. Gao and Z. Q. Li, "Thickness-dependent transport channels in topological insulator Bi2Se3 thin films grown by magnetron sputtering," *Scientific Reports,* vol. 6, p. 25291, 2016.

[48] P. Roushan, J. Seo, C. V. Parker, Y. S. Hor, D. Hsieh, D. Qian, A. Richardella, M. Z. Hasan, R. J. Cava and A. Yazdani, "Topological surface states protected from backscattering by chiral spin texture," *Nature,* vol. 460, p. 1106, 2009.

[49] J. Chen, H. J. Qin, F. Yang, J. Liu, T. Guan, F. M. Qu, G. H. Zhang, J. R. Shi, X. C. Xie, C. L. Yang, K. H. Wu, Y. Q. Li and L. Lu, "Gate-Voltage Control of Chemical Potential and Weak Antilocalization in Bi2Se3," *Phys. Rev. Lett.,* vol. 105, p. 176602, 2010.

[50] M.-X. Wang, C. Liu, J.-P. Xu, F. Yang, L. Miao, M.-Y. Yao, C. L. Gao, C. Shen, X. Ma, X. Chen, Z.-A. Xu, Y. Liu, S.-C. Zhang, D. Qian, J.-F. Jia and Q.-K. Xue, "The Coexistence of Superconductivity and Topological Order in the Bi2Se3 Thin Films," *Science,* vol. 336, pp. 52-55, 2012.

[51] L. Fu and C. L. Kane, "Superconducting proximity effect and Majorana fermions at the surface of a topological insulator," *Phys Rev Lett,* vol. 100, p. 096407, 2008.

[52] F. Katmis, V. Lauter, F. S. Nogueira, B. A. Assaf, M. E. Jamer, P. Wei, B. Satpati, J. W. Freeland, I. Eremin, D. Heiman, P. Jarillo-Herrero and J. S. Moodera, "A high-temperature ferromagnetic topological insulating phase by proximity coupling," *Nature,* vol. 533, pp. 513-516, 2016.

[53] C. Chang, J. Zhang, X. Feng, J. Shen, Z. Zhang, M. Guo, K. Li, Y. Ou, P. Wei, L. Wang, Z. Ji, Y. Feng, S. Ji, X. Chen, J. Jia, X. Dai, Z. Fang, S.-. ZHang, K. He, Y. Wang, L. Lu, X. Ma and Q. Xue, "Experimental Observation of the Quantum Anomalous Hall Effect in a Magnetic Topological Insulator," *Science,* vol. 340, p. 167, 2013.

[54] R. Yu, W. Zhang, H.-J. Zhang, S.-C. Zhang, X. Dai and Z. Fang, "Quantized Anomalous Hall Effect in Magnetic Topological Insulators," *Science,* vol. 329, p. 61, 2010.

[55] C.-X. Liu, H. Zhang, B. Yan, X.-L. Qi, T. Frauenheim, X. Dai, Z. Fang and S.-C. Zhang, "Oscillatory crossover from two-dimensional to three-dimensional topological insulators," *Phys. Rev. B.,* vol. 81, p. 041307(R), 2010.

[56] H.-Z. Lu, W.-Y. Shan, W. Yao, Q. Niu and S.-Q. Shen, "Massive Dirac fermions and spin physics in an ultrathin film of topological insulator," *Phys.Rev. B.,* vol. 81, p. 115407, 2010.

[57] J. Linder, T. Yokoyama and A. Subdo, "Anomalous finite size effects on surface states in the topological insulator Bi2Se3," *Phys. Rev. B.,* vol. 80, p. 205401, 2009.

[58] M. Neupane, A. Richardella, J. Sa´nchez-Barriga, S. Y. Xu, N. Alidoust, I. Belopolski, C. Liu, G. Bian, D. Zhang, D. Marchenko, A. Varykhalov, O. Rader, M. Leandersson, T. Balasubramanian, T. R. Chang, H. T. Jeng, S. Basak, H. Lin, A. Bansil, M. Samarth and M. Z. Hasan, "Observation of quantum-tunnelling-modulated spin testure in ultrathin topological insulator Bi2Se3 films," *Nature Communications,* vol. 5, p. 3841, 2014.

[59] S. Cho, P. B. Nicholas, J. Paglione and M. S. Fuher, "Insulating Behavior in Ultrathin Bismuth Selenide Field Effect Transistors," *NaNo Letters,* vol. 11, pp. 1925-1927, 2011.

[60] J. Sun and D. J. Sing, "Using gapped topological surface states of Bi2Se3 in a field effect transistor," *J. App. Phys.,* vol. 121, p. 064301, 2017.

[61] H. Cao, R. Venkatasubramanian, C. Liu, J. Pierce , H. Yang, M. Z. Hasan, Y. Wu and Y. P. Chen, "Topological insulator Bi2Te3 films synthesized by metal organic chemical vapor deposition," *Appl. Phys. Lett.,* vol. 101, p. 162104, 2012.

[62] A. Vargas, S. Basak, F. Liu, B. Wang, E. Panaitescu, H. Lin, R. Markiewicz, A. Bansil and S. Kar, "The Changing Colors of a Quantum-Confined Topological Insulator," *ACS NaNo,* vol. 8, p. 1222–1230, 2014.

[63] A. Richardella, D. M. Zhang, J. S. Lee, A. Koser, D. W. Rench, A. L. Yeats, B. B. Buckley, D. D. Awschalom and N. Samarth, "Coherent heteroepitaxy of Bi2Se3Bi2Se3 on GaAs (111)B," *Appl. Phys. Lett.* , vol. 97, p. 262104, 2011.

[64] N. Bansal, Y. S. Kim, E. Edrey, M. Brahlek, Y. Horibe, K. Lida, M. Tanimura, G.-H. Li, T. Feng, H.-D. Lee, T. Gustafsson and E. Andrei, "Epitaxial growth of topological insulator Bi2Se3 film on Si(111) with atomically sharp interface," *Thin Solid Films,* vol. 520, pp. 224-229, 2011.

[65] H. D. Li, Z. Y. Wang, X. Kan, X. Guo, H. T. He, Z. Wang, J. N. Wang, T. L. Wong, N. Wang and M. H. Xie, "The van der Waals epitaxy of Bi2Se3 on the vicinal Si(111) surface: an approach for preparing high-quality thin films of a topological insulator.," *New Journal of Physics,* vol. 12, p. 103038, 2010.

[66] C. Song, Y. Wang, X. Zhang, C. Chang, L. Wang, K. He, X. Chen, J. Jia, Y. Wang, Z. Fang, X. Dai, X. Xie, X. Qi, S. Zhang and Q. Xue, "Topological Insulator Bi2Se3 thinfilms grwon on double-layer graphene by molecular beam epitaxy," *Applied Physics letters,* vol. 97, p. 143118, 2010.

[67] A. A. Taskin, S. Sasaki, K. Segawa and Y. Ando, "Manifestation of Topological Protection in Transport Properties of Epitaxial Bi2Se3," *Phys. Rev. Lett.,* vol. 109, p. 066803, 2012.

[68] S. Schreyeck, N. V. Tarakina, G. Karczewski, C. Schumacher, T. Borzenko, C. Brüne, H. Buhmann, C. Gould, K. Brunner and L. W. Molenkamp, "Molecular beam epitaxy of high structural quality Bi2Se3 on lattice matched InP(111) substrates," *Appl. Phys. Lett.,* vol. 102, p. 041914, 2013.

[69] X. F. Kou, F. X. Xiu, M. R. Lang, Z. M. Liao, Y. Wang, A. V. Fedorov, X. X. Yu, J. S. Tang, G. Huang, X. W. Jiang, J. F. Zhu, J. Zou and K. L. Wang, "Epitaxial growth of high mobility Bi2Se3 thin films on CdS," *Appl. Phys. Lett.,* vol. 98, p. 242102, 2011.

[70] W. J. Wang, K. H. Gao and Z. Q. Li, "Thickness-dependent transport channels in topological insulator bi2Se3 thin films grown by magnetron sputtering," *Scientiffic Reports,* vol. 6, p. 25291, 2016.

[71] K. Wasa and S. Hayakawa, Handbook of Sputter Deposition Technology, 1991.

[72] L. G. Parratt, "Surface Studies of Solids by Total Reflection of X-Rays," *Phys. Rev. Lett.,* vol. 95, p. 359, 1954.

[73] M. Björck and G. Andersson, "GenX: an extensible X-ray reflectivity refinement program utilizing differential evolution," *J. Appl. Crys.,* vol. 40, pp. 1174-1178, 2007.

[74] L. J. Van der Pauw, "A method of measuring specific resistivity and Hall effect of discs of arbitrary shape," *Phillipos Research Reports,* vol. 13, pp. 1-9, 1958.

[75] K. Momma and F. Izumi, "VESTA 3 for three-dimensional visualization of crystal, volumetric and morphology data," *J. Appl. Cryst.,* vol. 44, p. 1272, 2011.

[76] S. Nakajima, "The crystal structure of Bi2Te3−xSex," *Journal of Physics and Chemistry of Solids,* vol. 24, p. 479, 1963.

[77] M. Liu, C. Chang, Z. Zhang, Y. Zhang, W. Ruan, K. He, L. Wang, X. Chen, J. Jia, S. Zhang, Q. Xue, X. Ma and Y. Wang, "Electron interaction-driven insulating ground state in Bi2Se3 topological insulators in the two-dimensional limit," *Phys. Rev. B,* vol. 83, p. 165440, 2011.

[78] W. Liu, X. Peng, X. Wei, H. Yang, G. M. Stocks and J. Zhong, "Surface and substrate induced effects on thin films of the topological insulators Bi2Se3 and Bi2Te3," *Phys. Rev. B,* vol. 87, p. 205315, 2013.

[79] J. Betancourt, S. Li, X. Dang, J. D. Burton, E. Y. Tsymbal and J. P. Velev, "J. Betancourt, S. Li, X. Dang, J. D. Burton, E. Y. Tsymbal and J. P. Velev, "Complex band structure of topological insulator Bi2Se3," *Journal of Physics: Condensed Matter,* vol. 28, p. 395501, 2016.

[80] Y. Sakamoto, T. Hirahara, H. Miyazaki, S.-I. Kimura and S. Hasegawa, "Spectroscopic evidence of a topological quantum phase transition in ultrathin Bi2Se3 films," *Phys. Rev. B.,* vol. 81, p. 165432, 2010.

[81] Q. Yang, M. Dolev, L. Zhang, J. Zhao, A. D. Fried, E. Schemm, M. Liu, A. Palevski, A. F. Marshall, S. H. Risbud and A. Kapitulnik, "Emerging weak localization effects on a topological insulator-insulating ferromagnet (Bi2Se3-EuS) interface," *Phys. Rev. B,* vol. 88, p. 081407(R), 2013.

[82] K. Post, B. C. Chapler, L. He, X. Kou, K. Wang and D. N. Basov, "Thickness-dependent bulk electronic properties in Bi2Se3 thin films revealed by infrared spectroscopy," *Phys. Rev. B.,* vol. 88, p. 075121, 2013.

[83] M. Eddrief, F. Vidal and B. Gallas, "Optical properties of Bi2Se3: from bulk to ultrathin films," *J. Phys. D.,* vol. 49, p. 505304, 2016.

[84] J. Son, K. Banerjee, M. Brahlek, N. Koirala, S.-K. Lee, J.-H. Ahn, S. O. Oh and H. Yang, "Conductance modulation in topological insulator Bi2Se3 thin films with ionic liquid," *Appl. Phys. Lett.,* vol. 103, p. 213114, 2013.

[85] H. Peng, W. Dang, J. Cao, Y. Chen, D. Wu, W. Zheng, H. Li, Z.-X. Shen and Z. Liu, "Topological insulator nanostructures for near-infrared transparent flexible electrodes," *Nature Chemistry,* vol. 4, pp. 281-286, 2012.

[86] E. Burstein, "Anomalous optical absorption limit in InSb," *Phys. Rev. B,* vol. 93, p. 632, 1954.

[87] J. G. Analytis , J.-H. Chu, Y. Chen, F. Corredor, R. D. McDonald, Z. X. Shen and I. R. Fisher, "Bulk Fermi surface coexistence with Dirac surface state in Bi2Se3: A comparison of photoemission and Shubnikov-de Haas measurements," *Phys. Rev. B,* vol. 81, p. 205407, 2010.

VITA

Graduate School

Southern Illinois University

Yub Raj Sapkota

rajyub.sapkota86@gmail.com

Tribhuvan University, Nepal

B.Sc. , 2008

Tribhuvan University, Nepal

M. Sc., 2012

Thesis Title: PHYSICAL PROPERTIES OF TOPOLOGICAL INSULATOR BISMUTH SELENIDE THIN FILMS

Advisor: Dr. Dipanjan Mazumdar

Publications

1. Yub Raj Sapkota, Asma Alkabsh, Aaron Walber, Hassana Samassekou and Dipanjan Mazumdar, *Optical evidence for blue shift in topological insulator bismuth selenide in the few-layer limit*, Applied Physics Letters, Vol. 110, No. 181901,2017

2. Yub Raj Sapkota, and Dpanjan Mazumdar, Transport properties of topological insulator Bismuth selenide thin films: Approaching the two-dimensional limit.